EUROPEAN ORGANIZATION FOR NUCLEAR RESEARCH (CERN)

arXiv:1805.06759v3 [hep-ex] 21 Aug 2018

Measurement of CP asymmetries in two-body $B^0_{(s)}$-meson decays to charged pions and kaons

LHCb collaboration[†]

Abstract

The time-dependent CP asymmetries in $B^0 \to \pi^+\pi^-$ and $B^0_s \to K^+K^-$ decays are measured using a data sample of pp collisions corresponding to an integrated luminosity of $3.0\,\text{fb}^{-1}$, collected with the LHCb detector at centre-of-mass energies of 7 and 8 TeV. The same data sample is used to measure the time-integrated CP asymmetries in $B^0 \to K^+\pi^-$ and $B^0_s \to \pi^+K^-$ decays. The results are $C_{\pi^+\pi^-} = -0.34 \pm 0.06 \pm 0.01$, $S_{\pi^+\pi^-} = -0.63 \pm 0.05 \pm 0.01$, $C_{K^+K^-} = 0.20 \pm 0.06 \pm 0.02$, $S_{K^+K^-} = 0.18 \pm 0.06 \pm 0.02$, $A^{\Delta\Gamma}_{K^+K^-} = -0.79 \pm 0.07 \pm 0.10$, $A^{B^0}_{CP} = -0.084 \pm 0.004 \pm 0.003$, and $A^{B^0_s}_{CP} = 0.213 \pm 0.015 \pm 0.007$, where the first uncertainties are statistical and the second systematic. Evidence for CP violation is found in the $B^0_s \to K^+K^-$ decay for the first time.

[†]Authors are listed at the end of this paper.

1   Introduction

The study of CP violation in charmless decays of $B^0_{(s)}$ mesons to charged two-body final states represents a powerful tool to test the Cabibbo-Kobayashi-Maskawa (CKM) picture [1, 2] of the quark-flavour mixing in the Standard Model (SM) and to investigate the presence of physics lying beyond [3–9]. As discussed in Refs. [5, 8, 9], the hadronic parameters entering the $B^0 \rightarrow \pi^+\pi^-$ and $B^0_s \rightarrow K^+K^-$ decay amplitudes are related by U-spin symmetry, *i.e.* by the exchange of d and s quarks in the decay diagrams.[1] It has been shown that a combined analysis of the branching fractions and CP asymmetries in two-body B-meson decays, accounting for U-spin breaking effects, allows stringent constraints on the CKM angle γ and on the CP-violating phase $-2\beta_s$ to be set [10, 11]. More recently, it has been proposed to combine the CP asymmetries of the $B^0 \rightarrow \pi^+\pi^-$ and $B^0_s \rightarrow K^+K^-$ decays with information provided by the semileptonic decays $B^0 \rightarrow \pi^-\ell^+\nu$ and $B^0_s \rightarrow K^-\ell^+\nu$, in order to achieve a substantial reduction of the theoretical uncertainty on the determination of $-2\beta_s$ [12, 13]. The CP asymmetry in the $B^0 \rightarrow \pi^+\pi^-$ decay is also a relevant input to the determination of the CKM angle α, when combined with other measurements from the isospin-related decays $B^0 \rightarrow \pi^0\pi^0$ and $B^+ \rightarrow \pi^+\pi^0$ [14–16].

In this paper, measurements of the time-dependent CP asymmetries in $B^0 \rightarrow \pi^+\pi^-$ and $B^0_s \rightarrow K^+K^-$ decays and of the time-integrated CP asymmetries in $B^0 \rightarrow K^+\pi^-$ and $B^0_s \rightarrow \pi^+K^-$ decays are presented. The analysis is based on a data sample of pp collisions corresponding to an integrated luminosity of $3.0\,\mathrm{fb}^{-1}$, collected with the LHCb detector at centre-of-mass energies of 7 and 8 TeV. The results supersede those from previous analyses performed with $1.0\,\mathrm{fb}^{-1}$ of integrated luminosity at LHCb [17, 18].

Assuming CPT invariance, the CP asymmetry as a function of decay time for $B^0_{(s)}$ mesons decaying to a CP eigenstate f is given by

$$A_{CP}(t) = \frac{\Gamma_{\overline{B}^0_{(s)} \rightarrow f}(t) - \Gamma_{B^0_{(s)} \rightarrow f}(t)}{\Gamma_{\overline{B}^0_{(s)} \rightarrow f}(t) + \Gamma_{B^0_{(s)} \rightarrow f}(t)} = \frac{-C_f \cos(\Delta m_{d,s} t) + S_f \sin(\Delta m_{d,s} t)}{\cosh\left(\frac{\Delta\Gamma_{d,s}}{2}t\right) + A^{\Delta\Gamma}_f \sinh\left(\frac{\Delta\Gamma_{d,s}}{2}t\right)}, \quad (1)$$

where $\Delta m_{d,s}$ and $\Delta\Gamma_{d,s}$ are the mass and width differences of the mass eigenstates in the $B^0_{(s)} - \overline{B}^0_{(s)}$ system. The quantities C_f, S_f and $A^{\Delta\Gamma}_f$ are defined as

$$C_f \equiv \frac{1 - |\lambda_f|^2}{1 + |\lambda_f|^2}, \qquad S_f \equiv \frac{2\mathrm{Im}\lambda_f}{1 + |\lambda_f|^2}, \qquad A^{\Delta\Gamma}_f \equiv -\frac{2\mathrm{Re}\lambda_f}{1 + |\lambda_f|^2}, \quad (2)$$

where λ_f is given by

$$\lambda_f \equiv \frac{q}{p}\frac{\overline{A}_f}{A_f}. \quad (3)$$

The two mass eigenstates of the effective Hamiltonian in the $B^0_{(s)} - \overline{B}^0_{(s)}$ system are $p|B^0_{(s)}\rangle \pm q|\overline{B}^0_{(s)}\rangle$, where p and q are complex parameters. The parameter λ_f is thus related to $B^0_{(s)} - \overline{B}^0_{(s)}$ mixing (via q/p) and to the decay amplitudes of the $B^0_{(s)} \rightarrow f$ decay (A_f) and of the $\overline{B}^0_{(s)} \rightarrow f$ decay ($\overline{A}_f$). Assuming negligible CP violation in the mixing ($|q/p| = 1$), as expected in the SM and confirmed by current experimental determinations [19–21], the terms C_f and S_f parameterise CP violation in the decay and in the interference

---

[1]Unless stated otherwise, the inclusion of charge-conjugate decay modes is implied throughout this paper.

Table 1: Current experimental knowledge on $C_{\pi^+\pi^-}$, $S_{\pi^+\pi^-}$, $C_{K^+K^-}$ and $S_{K^+K^-}$. For the experimental measurements, the first uncertainties are statistical and the second systematic, whereas for the averages the uncertainties include both contributions. The correlation factors, denoted as ρ, are also reported.

Reference	$C_{\pi^+\pi^-}$	$S_{\pi^+\pi^-}$	$\rho\left(C_{\pi^+\pi^-},\, S_{\pi^+\pi^-}\right)$
BaBar [22]	$-0.25 \pm 0.08 \pm 0.02$	$-0.68 \pm 0.10 \pm 0.03$	-0.06
Belle [23]	$-0.33 \pm 0.06 \pm 0.03$	$-0.64 \pm 0.08 \pm 0.03$	-0.10
LHCb [17]	$-0.38 \pm 0.15 \pm 0.02$	$-0.71 \pm 0.13 \pm 0.02$	0.38
HFLAV average [19]	-0.31 ± 0.05	-0.66 ± 0.06	0.00
	$C_{K^+K^-}$	$S_{K^+K^-}$	$\rho\left(C_{K^+K^-},\, S_{K^+K^-}\right)$
LHCb [17]	$0.14 \pm 0.11 \pm 0.03$	$0.30 \pm 0.12 \pm 0.04$	0.02

Table 2: Current experimental knowledge on A_{CP} for $B^0 \to K^+\pi^-$ and $B_s^0 \to \pi^+K^-$ decays. For the experimental measurements, the first uncertainties are statistical and the second systematic, whereas for the averages the uncertainties include both contributions.

Experiment	$A_{CP}^{B^0}$	$A_{CP}^{B_s^0}$
BaBar [22]	$-0.107 \pm 0.016 \, ^{+\,0.006}_{-\,0.004}$	$-$
Belle [24]	$-0.069 \pm 0.014 \pm 0.007$	$-$
CDF [25]	$-0.083 \pm 0.013 \pm 0.004$	$0.22 \pm 0.07 \pm 0.02$
LHCb [18]	$-0.080 \pm 0.007 \pm 0.003$	$0.27 \pm 0.04 \pm 0.01$
HFLAV average [19]	-0.082 ± 0.006	0.26 ± 0.04

between mixing and decay, respectively. The quantities C_f, S_f and $A_f^{\Delta\Gamma}$ must satisfy the condition $\left(C_f\right)^2 + \left(S_f\right)^2 + \left(A_f^{\Delta\Gamma}\right)^2 = 1$. This constraint is not imposed in this analysis, but its validity is verified *a posteriori* as a cross-check. In this paper a negligible value of $\Delta\Gamma_d$ is assumed, as supported by current experimental knowledge [19]. Hence the expression of the time-dependent CP asymmetry for the $B^0 \to \pi^+\pi^-$ decay simplifies to $A_{CP}(t) = -C_{\pi^+\pi^-}\cos(\Delta m_d t) + S_{\pi^+\pi^-}\sin(\Delta m_d t)$. The time-integrated CP asymmetry for a $B_{(s)}^0$ decay to a flavour-specific final state f, such as $B^0 \to K^+\pi^-$ and $B_s^0 \to \pi^+K^-$, is defined as

$$A_{CP} = \frac{\left|\bar{A}_{\bar{f}}\right|^2 - \left|A_f\right|^2}{\left|\bar{A}_{\bar{f}}\right|^2 + \left|A_f\right|^2}, \tag{4}$$

where A_f $(\bar{A}_{\bar{f}})$ is the decay amplitude of the $B_{(s)}^0 \to f$ $(\bar{B}_{(s)}^0 \to \bar{f})$ transition. The current experimental knowledge on C_f and S_f for the $B^0 \to \pi^+\pi^-$ and $B_s^0 \to K^+K^-$ decays, and on A_{CP} for the $B^0 \to K^+\pi^-$ $(A_{CP}^{B^0})$ and $B_s^0 \to \pi^+K^-$ $(A_{CP}^{B_s^0})$ decays, is summarised in Tables 1 and 2, respectively. Only LHCb measured $C_{K^+K^-}$ and $S_{K^+K^-}$, while no previous measurement of $A_{K^+K^-}^{\Delta\Gamma}$ is available to date.

This paper is organised as follows. After a brief introduction to the LHCb detector, trigger and simulation in Sec. 2, the event selection is described in Sec. 3. The CP asymmetries are determined by means of a simultaneous unbinned maximum likelihood fit to the distributions of candidates reconstructed in the $\pi^+\pi^-$, K^+K^- and $K^+\pi^-$ final-state

hypotheses, with the fit model described in Sec. 4. The measurement of time-dependent CP asymmetries with $B_{(s)}^0$ mesons requires that the flavour of the decaying meson at the time of production is identified (flavour tagging), as discussed in Sec. 5. In Sec. 6, the procedure to calibrate the per-event decay-time uncertainty is presented. The determination of the detection asymmetry between the $K^+\pi^-$ and $K^-\pi^+$ final states, necessary to measure A_{CP}, is discussed in Sec. 7. The results of the fits are given in Sec. 8 and the assessment of systematic uncertainties in Sec. 9. Finally, conclusions are drawn in Sec. 10.

2   Detector, trigger and simulation

The LHCb detector [26, 27] is a single-arm forward spectrometer covering the pseudorapidity range $2 < \eta < 5$, designed for the study of particles containing b or c quarks. The detector includes a high-precision tracking system consisting of a silicon-strip vertex detector surrounding the pp interaction region, a large-area silicon-strip detector located upstream of a dipole magnet with a bending power of about $4\,\mathrm{Tm}$, and three stations of silicon-strip detectors and straw drift tubes placed downstream of the magnet. The tracking system provides a measurement of momentum, p, of charged particles with a relative uncertainty that varies from 0.5% at low momentum to 1.0% at $200\,\mathrm{GeV}/c$. The minimum distance of a track to a primary vertex (PV), the impact parameter (IP), is measured with a resolution of $(15 + 29/p_\mathrm{T})\,\mu\mathrm{m}$, where p_T is the component of the momentum transverse to the beam, in GeV/c. Different types of charged hadrons are distinguished using information from two ring-imaging Cherenkov (RICH) detectors. Photons, electrons and hadrons are identified by a calorimeter system consisting of scintillating-pad and preshower detectors, an electromagnetic calorimeter and a hadronic calorimeter. Muons are identified by a system composed of alternating layers of iron and multiwire proportional chambers. The online event selection is performed by a trigger [28], which consists of a hardware stage, based on information from the calorimeter and muon systems, followed by a software stage, which applies a full event reconstruction.

At the hardware trigger stage, events are required to have a muon with high p_T or a hadron, photon or electron with high transverse energy in the calorimeters. For hadrons, the transverse energy threshold is $3.5\,\mathrm{GeV}$. The software trigger requires a two-track secondary vertex with a significant displacement from the PVs. At least one charged particle must have a transverse momentum $p_\mathrm{T} > 1.7\,\mathrm{GeV}/c$ in the $7\,\mathrm{TeV}$ or $p_\mathrm{T} > 1.6\,\mathrm{GeV}/c$ in the $8\,\mathrm{TeV}$ data, and be inconsistent with originating from a PV. A multivariate algorithm [29] is used for the identification of secondary vertices consistent with the decay of a b hadron. In order to improve the efficiency on signal, a dedicated trigger selection for two-body b-hadron decays is implemented, imposing requirements on the quality of the reconstructed tracks, their p_T and IP, the distance of closest approach between the decay products, and the p_T, IP and proper decay time of the b-hadron candidate.

Simulation is used to study the discrimination between signal and background events, and to assess the small differences between signal and calibration decays. The pp collisions are generated using PYTHIA [30, 31] with a specific LHCb configuration [32]. Decays of hadronic particles are described by EvtGen [33], in which final-state radiation is generated using PHOTOS [34]. The interaction of the generated particles with the detector, and its response, are implemented using the GEANT4 toolkit [35] as described in Ref. [36].

3 Event selection

The candidates selected online by the trigger are filtered offline to reduce the amount of combinatorial background by means of a loose preselection. In addition, the decay products of the candidates, generically called B, are required either to be responsible for the positive decision of the hadronic hardware trigger, or to be unnecessary for an affirmative decision of any of the hardware trigger requirements. Candidates that pass the preselection are then classified into mutually exclusive samples of different final states ($\pi^+\pi^-$, K^+K^-, $K^+\pi^-$ and $K^-\pi^+$) by means of the particle identification (PID) capabilities of the LHCb detector. Finally, a boosted decision tree (BDT) algorithm [37,38] is used to separate signal from combinatorial background.

Three types of backgrounds are considered: other two-body b-hadron decays with misidentified pions, kaons or protons in the final state (cross-feed background); pairs of randomly associated, oppositely charged tracks (combinatorial background); and pairs of oppositely charged tracks from partially reconstructed three-body decays of b hadrons (three-body background). Since the three-body background gives rise to candidates with invariant-mass values well separated from the signal mass peak, the event selection is customised to reject mainly the cross-feed and combinatorial backgrounds, which affect the invariant mass region around the B^0 and B_s^0 masses.

The main cross-feed background in the $\pi^+\pi^-$ (K^+K^-) spectrum is the $B^0 \to K^+\pi^-$ decay, where a kaon (pion) is misidentified as a pion (kaon). The PID requirements are optimised in order to reduce the amount of this cross-feed background to approximately 10% of the $B^0 \to \pi^+\pi^-$ and $B_s^0 \to K^+K^-$ signals, respectively. The same strategy is adopted to optimise the PID requirements for the $K^+\pi^-$ final state, reducing the amount of the $B^0 \to \pi^+\pi^-$ and $B_s^0 \to K^+K^-$ cross-feed backgrounds to approximately 10% of the $B_s^0 \to \pi^+K^-$ yield. The PID efficiencies and misidentification probabilities for kaons and pions are determined using samples of $D^{*+} \to D^0(\to K^-\pi^+)\pi^+$ decays [39].

The BDT exploits the following properties of the decay products: the p_T of the two tracks; the minimum and maximum $\chi^2_{\rm IP}$ of the two tracks with respect to all primary vertices, where $\chi^2_{\rm IP}$ is defined as the difference in vertex-fit χ^2 of a given PV reconstructed with and without the considered particle; the distance of closest approach between the two tracks and the quality of their common vertex fit. The BDT also uses properties of the reconstructed B candidate, namely the p_T, the $\chi^2_{\rm IP}$ with respect to the associated PV,[2] and the χ^2 of the distance of flight with respect to the associated PV, for a total of 9 variables. A single BDT is used to select the four signal decay modes. This is trained with $B^0 \to \pi^+\pi^-$ simulated events to model the signal, and data in the high-mass sideband (from 5.6 to 5.8 GeV/c^2) of the $\pi^+\pi^-$ sample to model the combinatorial background. The possibility to use a different BDT selection for each signal has been investigated, finding no sizeable differences in the sensitivities on the CP-violating quantities under study. The optimal threshold on the BDT response is chosen to maximise $S/\sqrt{S+B}$, where S and B represent the estimated numbers of $B^0 \to \pi^+\pi^-$ signal and combinatorial background events, respectively, within ± 60 MeV/c^2 (corresponding to about ± 3 times the invariant mass resolution) around the B^0 mass. Multiple candidates are present in less than 0.05% of the events in the final sample. Only one candidate is accepted for each event on the basis of a reproducible pseudorandom sequence.

---

[2] The associated PV is that with the smallest $\chi^2_{\rm IP}$ with respect to the B candidate.

4 Fit model

For each signal and relevant background component, the distributions of invariant mass, decay time, flavour-tagging assignment with the associated mistag probability, and per-event decay-time uncertainty are modelled. The flavour-tagging assignment and its associated mistag probability are provided by two classes of algorithms, so-called opposite-side (OS) and same-side (SS) tagging, as discussed in Sec. 5. Hence for each component it is necessary to model two flavour-tagging decisions and the associated mistag probabilities.

Signals are the $B^0 \to K^+\pi^-$ and $B_s^0 \to \pi^+K^-$ decays in the $K^+\pi^-$ sample, the $B^0 \to \pi^+\pi^-$ decay in the $\pi^+\pi^-$ sample, and the $B_s^0 \to K^+K^-$ decay in the K^+K^- sample. In the $\pi^+\pi^-$ and K^+K^- samples, small but non-negligible components of $B_s^0 \to \pi^+\pi^-$ and $B^0 \to K^+K^-$ decays, respectively, are present and must be taken into account. Apart from the cross-feed backgrounds from B-meson decays considered in the optimisation of the event selection, the only other relevant source of cross-feed background is the $\Lambda_b^0 \to pK^-$ decay with the proton misidentified as a kaon in the K^+K^- sample. Considering the PID efficiencies, the branching fractions and the relative hadronisation probabilities [19], this background is expected to give a contribution of about 2.5% relative to the $B_s^0 \to K^+K^-$ decay. This component is also modelled in the fit. Two components of three-body backgrounds need to be modelled in the $K^+\pi^-$ sample: one due to B^0 and B^+ decays, and one due to B_s^0 decays. The only relevant contributions of three-body backgrounds to the $\pi^+\pi^-$ and K^+K^- samples are found to be B^0 and B^+ decays, and B_s^0 decays, respectively. Components describing the combinatorial background are necessary in all of the three final states.

4.1 Mass model

The signal component for each two-body decay is modelled by the probability density function (PDF) for the candidate mass m

$$\mathcal{P}_{\text{sig}}(m) = (1 - f_{\text{tail}})G(m; \mu, \sigma_1, \sigma_2, f_{\text{g}}) + f_{\text{tail}}J(m; \mu, \sigma_1, \alpha_1, \alpha_2), \tag{5}$$

where $G(m; \mu, \sigma_1, \sigma_2, f_{\text{g}})$ is the sum of two Gaussian functions with common mean μ and widths σ_1 and σ_2, respectively; f_{g} is the relative fraction between the two Gaussian functions; f_{tail} is the relative fraction of the Johnson function $J(m; \mu, \sigma_1, \alpha_1, \alpha_2)$, defined as [40]

$$J(m; \mu, \sigma_1, \alpha_1, \alpha_2) = \frac{\alpha_2}{\sigma_1\sqrt{2\pi(1 + z^2)}} \exp\left[-\frac{1}{2}\left(\alpha_1 + \alpha_2 \sinh^{-1} z\right)^2\right], \tag{6}$$

where $z \equiv \left[\frac{m-\mu}{\sigma_1}\right]$, μ and σ_1 are in common with the dominant Gaussian function in Eq. (5), and α_1 and α_2 are two parameters governing the left- and right-hand side tails. In the fit to data, the parameters α_1, α_2 and f_{tail} are fixed to the values determined by fitting the model to samples of simulated decays, whereas the other parameters are left free to be adjusted by the fit.

The invariant-mass model of the cross-feed backgrounds is based on a kernel estimation method [41] applied to simulated decays. The amount of each cross-feed background component is determined by rescaling the yields of the decay in the correct spectrum by the ratio of PID efficiencies for the correct and wrong mass hypotheses. For example,

the yields of the $B^0 \to K^+\pi^-$ decay in the $\pi^+\pi^-$ spectrum are determined through the equation

$$N_{\pi^+\pi^-}(B^0 \to K^+\pi^-) = N(B^0 \to K^+\pi^-)\ \frac{\varepsilon_{\pi^+\pi^-}(B^0 \to K^+\pi^-)}{\varepsilon_{K^+\pi^-}(B^0 \to K^+\pi^-)}, \tag{7}$$

where $N_{\pi^+\pi^-}(B^0 \to K^+\pi^-)$ is the number of $B^0 \to K^+\pi^-$ decays present in the $\pi^+\pi^-$ sample, $N(B^0 \to K^+\pi^-)$ is the number of $B^0 \to K^+\pi^-$ decays identified in the $K^+\pi^-$ sample, $\varepsilon_{\pi^+\pi^-}(B^0 \to K^+\pi^-)$ is the probability to assign the $\pi^+\pi^-$ hypothesis to a $B^0 \to K^+\pi^-$ decay, and $\varepsilon_{K^+\pi^-}(B^0 \to K^+\pi^-)$ is the probability to assign the correct hypothesis to a $B^0 \to K^+\pi^-$ decay.

The components due to three-body B decays are described by convolving a sum of two Gaussian functions, defined using the same parameters as those used in the signal model, with ARGUS functions [42]. For the $K^+\pi^-$ sample two three-body background components are used: one describing three-body B^0 and B^+ decays and one describing three-body B_s^0 decays. For the $\pi^+\pi^-$ and K^+K^- samples a single ARGUS component is found to be sufficient to describe the invariant-mass shape in the low-mass region. The combinatorial background is modelled by exponential functions with an independent slope for each final-state hypothesis.

4.2   Decay-time model

The time-dependent decay rate of a flavour-specific $B \to f$ decay and of its CP conjugate $\bar{B} \to \bar{f}$, as for the cases of $B^0 \to K^+\pi^-$ and $B_s^0 \to \pi^+K^-$ decays, is given by the PDF

$$\begin{aligned}
f_{\mathrm{FS}}\left(t, \delta_t, \psi, \vec{\xi}, \vec{\eta}\right) = &K_{\mathrm{FS}}\left(1 - \psi A_{CP}\right)\left(1 - \psi A_{\mathrm{F}}\right) \times \\
&\left\{\left[(1-A_{\mathrm{P}})\Omega_{\mathrm{sig}}(\vec{\xi},\vec{\eta}) + (1+A_{\mathrm{P}})\bar{\Omega}_{\mathrm{sig}}(\vec{\xi},\vec{\eta})\right]H_+\left(t, \delta_t\right) + \right. \tag{8}\\
&\left. \psi\left[(1-A_{\mathrm{P}})\Omega_{\mathrm{sig}}(\vec{\xi},\vec{\eta}) - (1+A_{\mathrm{P}})\bar{\Omega}_{\mathrm{sig}}(\vec{\xi},\vec{\eta})\right]H_-\left(t, \delta_t\right)\right\},
\end{aligned}$$

where K_{FS} is a normalisation factor and the discrete variable ψ assumes the value $+1$ for the final state f and -1 for the final state $\bar{f}$. The direct CP asymmetry, A_{CP}, is defined in Eq. (4), while the final-state detection asymmetry, A_{F}, and the $B_{(s)}^0$-meson production asymmetry, A_{P}, are defined as

$$A_{\mathrm{F}} = \frac{\varepsilon_{\mathrm{tot}}\left(\bar{f}\right) - \varepsilon_{\mathrm{tot}}\left(f\right)}{\varepsilon_{\mathrm{tot}}\left(\bar{f}\right) + \varepsilon_{\mathrm{tot}}\left(f\right)}, \qquad A_{\mathrm{P}} = \frac{\sigma_{B_{(s)}^0} - \sigma_{\bar{B}_{(s)}^0}}{\sigma_{B_{(s)}^0} + \sigma_{\bar{B}_{(s)}^0}}, \tag{9}$$

where $\varepsilon_{\mathrm{tot}}$ is the time-integrated efficiency in reconstructing and selecting the final state f or $\bar{f}$, and $\sigma_{B_{(s)}^0}$ ($\sigma_{\bar{B}_{(s)}^0}$) is the production cross-section of the given $B_{(s)}^0$ ($\bar{B}_{(s)}^0$) meson. The asymmetry A_{P} arises because production rates of $B_{(s)}^0$ and $\bar{B}_{(s)}^0$ mesons are not expected to be identical in proton-proton collisions. It is measured to be order of percent at LHC energies [43]. Although A_{CP} can be determined from a time-integrated analysis, its value needs to be disentangled from the contribution of the production asymmetry. By studying the more general time-dependent decay rate, the production asymmetry can be determined simultaneously.

The variable $\vec{\xi} = (\xi_{\mathrm{OS}}, \xi_{\mathrm{SS}})$ is the pair of flavour-tagging assignments of the OS and SS algorithms used to identify the $B_{(s)}^0$-meson flavour at production, and $\vec{\eta} = (\eta_{\mathrm{OS}}, \eta_{\mathrm{SS}})$ is

the pair of associated mistag probabilities defined in Sec. 5. The variables $\xi_{\rm OS}$ and $\xi_{\rm SS}$ can assume the discrete values $+1$ when the candidate is tagged as $B^0_{(s)}$, -1 when the candidate is tagged as $\overline{B}^0_{(s)}$, and zero for untagged candidates. The functions $\Omega_{\rm sig}(\vec{\xi},\vec{\eta})$ and $\bar{\Omega}_{\rm sig}(\vec{\xi},\vec{\eta})$ are the PDFs of the variables $\vec{\xi}$ and $\vec{\eta}$ for a $B^0_{(s)}$ or a $\overline{B}^0_{(s)}$ meson, respectively. Their definitions are given in Sec. 5. The functions $H_+(t,\delta_t)$ and $H_-(t,\delta_t)$ are defined as

$$
\begin{aligned}
H_+(t,\delta_t) &= \left[e^{-\Gamma_{d,s}t'}\cosh\left(\frac{\Delta\Gamma_{d,s}}{2}t'\right)\right] \otimes R\left(t-t'|\delta_t\right)\,g_{\rm sig}\left(\delta_t\right)\,\varepsilon_{\rm sig}\left(t\right), \qquad (10)\\
H_-(t,\delta_t) &= \left[e^{-\Gamma_{d,s}t'}\cos\left(\Delta m_{d,s}t'\right)\right] \otimes R\left(t-t'|\delta_t\right)\,g_{\rm sig}\left(\delta_t\right)\,\varepsilon_{\rm sig}\left(t\right),
\end{aligned}
$$

where $R\left(t-t'|\delta_t\right)$ and $g_{\rm sig}\left(\delta_t\right)$ are the decay-time resolution model and the PDF of the per-event decay-time uncertainty δ_t, respectively, discussed in Sec. 6, and $\varepsilon_{\rm sig}(t)$ is the time-dependent efficiency in reconstructing and selecting signal decays.

If the final state f is a CP eigenstate, as for the $B^0 \to \pi^+\pi^-$ and $B^0_s \to K^+K^-$ decays, the decay-time PDF is given by

$$
\begin{aligned}
f_{CP}\left(t,\delta_t,\vec{\xi},\vec{\eta}\right) = K_{CP} &\left\{\left[\left(1-A_{\rm P}\right)\Omega_{\rm sig}\left(\vec{\xi},\vec{\eta}\right) + \left(1+A_{\rm P}\right)\bar{\Omega}_{\rm sig}\left(\vec{\xi},\vec{\eta}\right)\right] I_+\left(t,\delta_t\right) +\right.\\
&\left.\left[\left(1-A_{\rm P}\right)\Omega_{\rm sig}\left(\vec{\xi},\vec{\eta}\right) - \left(1+A_{\rm P}\right)\bar{\Omega}_{\rm sig}\left(\vec{\xi},\vec{\eta}\right)\right] I_-\left(t,\delta_t\right)\right\},
\end{aligned}
\qquad (11)
$$

where K_{CP} is a normalisation factor and the functions $I_+(t)$ and $I_-(t)$ are

$$
\begin{aligned}
I_+(t,\delta_t) &= \left\{e^{-\Gamma_{d,s}t'}\left[\cosh\left(\frac{\Delta\Gamma_{d,s}}{2}t'\right) + A_f^{\Delta\Gamma}\sinh\left(\frac{\Delta\Gamma_{d,s}}{2}t'\right)\right]\right\} \otimes \\
&\qquad R\left(t-t'|\delta_t\right)\,g_{\rm sig}\left(\delta_t\right)\,\varepsilon_{\rm sig}\left(t\right),\\
I_-(t,\delta_t) &= \left\{e^{-\Gamma_{d,s}t'}\left[C_f\cos\left(\Delta m_{d,s}t'\right) - S_f\sin\left(\Delta m_{d,s}t'\right)\right]\right\} \otimes \\
&\qquad R\left(t-t'|\delta_t\right)\,g_{\rm sig}\left(\delta_t\right)\,\varepsilon_{\rm sig}\left(t\right).
\end{aligned}
\qquad (12)
$$

It is instructive to see how the equations above would become in the absence of experimental effects. The final-state detection asymmetry $A_{\rm F}$ would have a zero value. In the limit of perfect flavour tagging, $i.e.$ absence of untagged candidates and mistag probabilities equal to zero with full agreement between OS and SS taggers, the function $\Omega_{\rm sig}(\vec{\xi},\vec{\eta})$ ($\bar{\Omega}_{\rm sig}(\vec{\xi},\vec{\eta})$) would become identically equal to 1 (0) if $\xi_{\rm OS,SS} = 1$, and to 0 (1) if $\xi_{\rm OS,SS} = -1$. The case of perfect determination of the decay time would be obtained by replacing the product of functions $R\left(t-t'|\delta_t\right)\,g_{\rm sig}\left(\delta_t\right)$ with a product of Dirac delta functions, $\delta(t-t')\,\delta(\delta_t)$. Finally, in the absence of a time dependence of the efficiency, the function $\varepsilon_{\rm sig}(t)$ would assume constant value.

The expressions for the decay-time PDFs of the cross-feed background components are determined from Eqs. (8) and (11), assuming that the decay time calculated under the wrong mass hypothesis is equal to that calculated using the correct hypothesis. This assumption is verified using samples of simulated decays.

The efficiency $\varepsilon_{\rm sig}(t)$ is parameterised using the empirical function

$$
\varepsilon_{\rm sig}\left(t\right) \propto \left[d_0 - {\rm erf}\left(d_1 t^{d_2}\right)\right]\left(1 - d_3 t\right),
\qquad (13)
$$

where erf denotes the error function and d_i are parameters determined using the $B^0 \to K^+\pi^-$ decay, whose untagged time-dependent decay rate is a pure exponential with

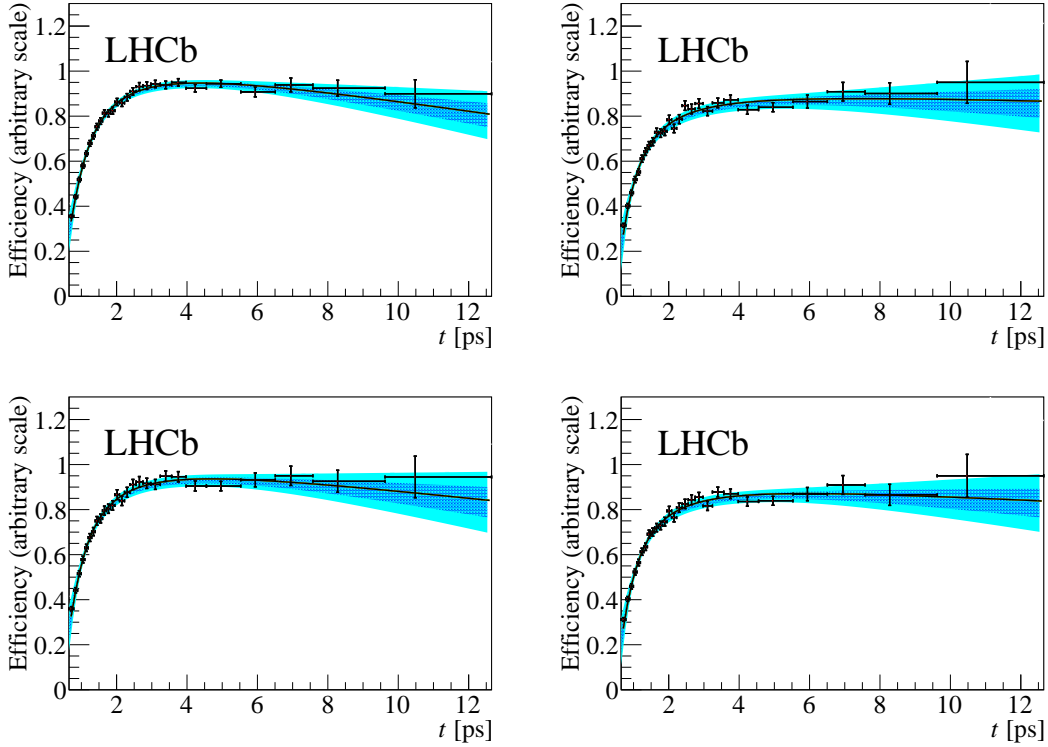Figure 1: Efficiencies as a function of decay time for (top left) $B^0 \to K^+\pi^-$, (top right) $B^0_s \to \pi^+K^-$, (bottom left) $B^0 \to \pi^+\pi^-$ and (bottom right) $B^0_s \to K^+K^-$ decays. The black line is the result of the best fit of Eq. (13) to the histograms, obtained as described in the text. The dark and bright areas correspond to the 68% and 95% confidence intervals, respectively.

$\Gamma_d = 0.6588 \pm 0.0017\,\text{ps}^{-1}$ [19]. The yield of the $B^0 \to K^+\pi^-$ decay is determined in bins of decay time, by means of unbinned maximum likelihood fits to the $K^+\pi^-$ invariant-mass spectrum, using the model described in Sec. 4.1. The resulting histogram is then divided by a histogram built from an exponential function with decay constant equal to the central value of Γ_d and arbitrary normalisation. By fitting the function in Eq. (13) to the final histogram, the parameters d_i are determined and fixed in the final fit to the data. The absolute scale of the efficiency function in Eq. (13) is irrelevant in the likelihood maximisation since its value is absorbed into the global normalisation of the PDFs. For the other two-body decays under study, the same efficiency histogram is used, but with a small correction in order to take into account the differences between the various decay modes. The correction consists in multiplying the histogram by the ratio between the time-dependent efficiencies for the $B^0 \to K^+\pi^-$ and the other modes, as determined from simulated decays. The final histograms and corresponding time-dependent efficiencies for the $B^0 \to K^+\pi^-$, $B^0_s \to \pi^+K^-$, $B^0 \to \pi^+\pi^-$ and $B^0_s \to K^+K^-$ decays are reported in Fig. 1.

The parameterisation of the decay-time distribution for combinatorial background in the $K^+\pi^-$ sample is studied by using the high-mass sideband from data, defined as

$5.6 < m < 5.8\,\mathrm{GeV}/c^2$. It is empirically found that the PDF can be written as

$$
\begin{aligned}
f_{\mathrm{comb}}\left(t, \delta_t, \psi, \vec{\xi}, \vec{\eta}\right) = {}& K_{\mathrm{comb}}\left(1 - \psi A_{\mathrm{comb}}\right)\Omega_{\mathrm{comb}}(\vec{\xi}, \vec{\eta})\,g_{\mathrm{comb}}(\delta_t) \times \\
& \left[f_{\mathrm{comb}}\,e^{-\Gamma_{\mathrm{comb}}t} + (1 - f_{\mathrm{comb}})\,e^{-\Gamma'_{\mathrm{comb}}t}\right]\varepsilon_{\mathrm{comb}}(t),
\end{aligned}
\tag{14}
$$

where K_{comb} is a normalisation factor; $\Omega_{\mathrm{comb}}(\vec{\xi}, \vec{\eta})$ is the PDF of $\vec{\xi}$ and $\vec{\eta}$ for combinatorial-background candidates; $g_{\mathrm{comb}}(\delta_t)$ is the distribution of the per-event decay-time uncertainty δ_t for combinatorial background, discussed in Sec. 6; A_{comb} is the charge asymmetry of the combinatorial background; and Γ_{comb}, Γ'_{comb} and f_{comb} are free parameters to be determined by the fit. The function $\varepsilon_{\mathrm{comb}}(t)$ is an effective function, analogous to the time-dependent efficiency for signal decays. The parameterisation

$$
\varepsilon_{\mathrm{comb}}(t) \propto 1 - \mathrm{erf}\left(\frac{a_{\mathrm{comb}} - t}{a_{\mathrm{comb}}t}\right),
\tag{15}
$$

where a_{comb} is a free parameter, provides a good description of the data. For the $\pi^+\pi^-$ and K^+K^- samples, the same expression as in Eq. (14) is used, with A_{comb} set to zero.

The decay-time distribution of the three-body background component in the $K^+\pi^-$ sample is described using the same PDF as in Eq. (8), but with independent parameters entering the flavour-tagging PDF and an independent effective oscillation frequency. In addition, the time-dependent efficiency function in Eq. (10) is parameterised as $\varepsilon_{\mathrm{sig}}(t) = \sum_{i=0}^{6} c_i b_i(t)$, following the procedure outlined in Ref. [44], where $b_i(t)$ are cubic spline functions and c_i are coefficients left free to be adjusted during the final fit to data.

For the $\pi^+\pi^-$ and K^+K^- samples, the decay-time distribution of three-body partially reconstructed backgrounds is parameterised using the PDF

$$
f_{\mathrm{3\text{-}body}}\left(t, \delta_t, \vec{\xi}, \vec{\eta}\right) = K_{\mathrm{3\text{-}body}}\,\Omega_{\mathrm{3\text{-}body}}(\vec{\xi}, \vec{\eta})\,g_{\mathrm{3\text{-}body}}(\delta_t)\,e^{-\Gamma_{\mathrm{3\text{-}body}}t}\varepsilon_{\mathrm{3\text{-}body}}(t),
\tag{16}
$$

where $K_{\mathrm{3\text{-}body}}$ is a normalisation factor, and $\Omega_{\mathrm{3\text{-}body}}(\vec{\xi}, \vec{\eta})$ and $g_{\mathrm{3\text{-}body}}(\delta_t)$ are the analogues of $\Omega_{\mathrm{comb}}(\vec{\xi}, \vec{\eta})$ and $g_{\mathrm{comb}}(\delta_t)$ of Eq. (14), respectively. The function $\varepsilon_{\mathrm{3\text{-}body}}(t)$ is parameterised as in Eq. (15), with an independent parameter $a_{\mathrm{3\text{-}body}}$, instead of a_{comb}, left free to be adjusted by the fit.

5 Flavour tagging

Flavour tagging is a fundamental ingredient to measure CP asymmetries with $B^0_{(s)}$-meson decays to CP eigenstates. The sensitivity to the coefficients C_f and S_f governing the time-dependent CP asymmetry defined in Eq. (1) is directly related to the tagging power, defined as $\varepsilon_{\mathrm{eff}} = \sum_i |\xi_i|\,(1 - 2\eta_i)^2/N$, where ξ_i and η_i are the tagging decision and the associated mistag probability, respectively, for the i-th of the N candidates.

Two classes of algorithms (OS and SS) are used to determine the initial flavour of the signal $B^0_{(s)}$ meson. The OS taggers [45] exploit the fact that in pp collisions beauty quarks are almost exclusively produced in $b\bar{b}$ pairs. Hence the flavour of the decaying signal $B^0_{(s)}$ meson can be determined by looking at the charge of the lepton, either muon or electron, originating from semileptonic decays, and of the kaon from the $b \to c \to s$ decay transition of the other b hadron in the event. An additional OS tagger is based on

the inclusive reconstruction of the opposite b-hadron decay vertex and on the computation of a p_{T}-weighted average of the charges of all tracks associated to that vertex. For each OS tagger, the probability of misidentifying the flavour of the $B^0_{(s)}$ meson at production (mistag probability, η) is estimated by means of an artificial neural network, and is defined in the range $0 \leq \eta \leq 0.5$. When the response of more than one OS tagger is available per candidate, the different decisions and associated mistag probabilities are combined into a unique decision ξ_{OS} and a single η_{OS}. The SS taggers are based on the identification of the particles produced in the hadronisation of the beauty quarks. In contrast to OS taggers, that to a very good approximation act equally on B^0 and B^0_s mesons, SS taggers are specific to the nature of the $B^0_{(s)}$ meson under study. The additional $\overline{d}$ (d) or $\overline{s}$ (s) quarks produced in association with a B^0 ($\overline{B}^0$) or a B^0_s ($\overline{B}^0_s$) meson, respectively, can form charged pions and protons, in the d-quark case, or charged kaons, in the s-quark case. In this paper, so-called SSπ and SSp taggers [46] are used to determine the initial flavour of B^0 mesons, while the SSK tagger [47] is used for B^0_s mesons.

The multivariate algorithms used to determine the values of η_{OS} and η_{SS} are trained using specific B-meson decay channels and selections. The differences between the training samples and the selected signal $B^0_{(s)}$ mesons can lead to an imperfect determination of the mistag probability. Hence, a more accurate estimate, denoted as ω hereafter, is obtained by means of a calibration procedure that takes into account the specific kinematics of selected signal $B^0_{(s)}$ mesons. In the OS case, the relation between η and ω is calibrated using $B^0 \to K^+\pi^-$ and $B^0_s \to \pi^+K^-$ decays. In the SSπ and SSp cases, only $B^0 \to K^+\pi^-$ decays are used. Once the calibration procedure is applied, the information provided by the two taggers is combined into a unique tagger, SSc, with decision ξ_{SSc} and mistag probability η_{SSc}, as discussed in App. A.2. In the SSK case, the small yield of the $B^0_s \to \pi^+K^-$ decay is insufficient for a precise calibration. Hence, a large sample of $B^0_s \to D^-_s\pi^+$ decays is used instead. The procedure is described in App. A.3.

Flavour-tagging information enters the PDF describing the decay-time distribution of the signals by means of the $\Omega_{\mathrm{sig}}(\vec{\xi}, \vec{\eta})$ and $\overline{\Omega}_{\mathrm{sig}}(\vec{\xi}, \vec{\eta})$ PDFs in Eqs. (8) and (11), and the same parameterisation is also adopted for the cross-feed backgrounds. Similar PDFs are used also for the combinatorial and three-body backgrounds. The full description of these PDFs is given in App. A, together with the details and the results of the calibration procedure.

6 Decay-time resolution

The model to describe the decay-time resolution is obtained from the study of signal and $B^0_s \to D^-_s\pi^+$ decays in simulation. It is found that the resolution function $R\left(t - t'|\delta_t\right)$ is well described by the sum of two Gaussian functions with a shared mean fixed to zero and widths that depend on the decay-time uncertainty δ_t, which varies on a candidate-by-candidate basis. The value of δ_t is determined for each B candidate by combining the information of momentum, invariant mass, decay length and their corresponding uncertainties. The two widths are parameterised as

$$
\begin{aligned}
\sigma_1(\delta_t) &= q_0 + q_1\,(\delta_t - \hat{\delta}_t), \\
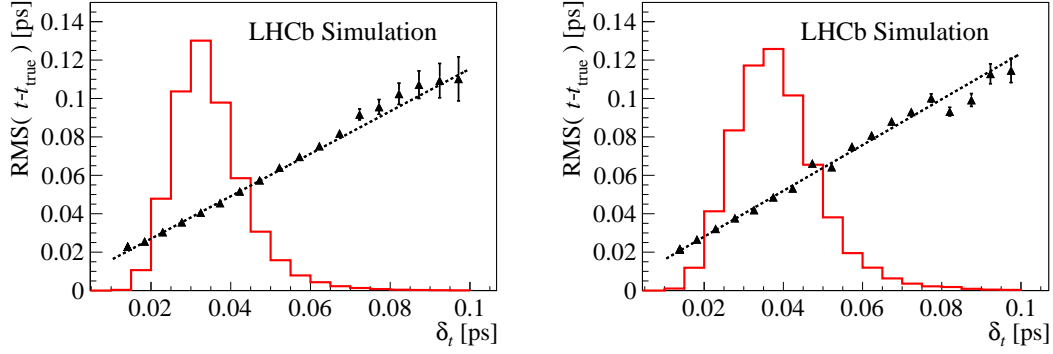\sigma_2(\delta_t) &= r_\sigma\,\sigma_1(\delta_t),
\end{aligned}
\tag{17}
$$

Figure 2: The triangles represent the standard deviation of the difference between the reconstructed (t) and true decay (t_{true}) time versus δ_t for simulated (left) $B_s^0 \to \pi^+ K^-$ and (right) $B_s^0 \to D_s^- \pi^+$ decays. The dotted lines are the results of linear-function fits. The histograms represent the corresponding δ_t distributions with arbitrary normalisations.

where $\hat{\delta}_t = 30\,\text{fs}$ is approximately equal to the mean value of the δ_t distribution. It is also found that the parameters q_0, q_1, r_σ and the relative fraction of the two Gaussian functions are very similar between signal and $B_s^0 \to D_s^- \pi^+$ decays. However, the simulation also shows the presence of a small component with long tails, that could be accommodated with a third Gaussian function with larger width. For simplicity the double Gaussian function is used in the baseline model, and a systematic uncertainty associated with this approximation is discussed in Sec. 9. Figure 2 shows the dependence on δ_t of the standard deviation of the difference between the reconstructed and true decay time for simulated $B_s^0 \to \pi^+ K^-$ and $B_s^0 \to D_s^- \pi^+$ decays. This dependence is found to be well modelled by a straight line. The parameter r_σ and the relative contribution of the first Gaussian function are fixed to 3.0 and 0.97, respectively, as determined from full simulation. The values of the parameters q_0 and q_1 are determined from data by means of OS-tagged time-dependent fits to a sample of $B_s^0 \to D_s^- \pi^+$ decays, where the combined response of the OS taggers is calibrated using a sample of $B^0 \to D^- \pi^+$ decays. Figure 3 shows the time-dependent asymmetries of the $B^0 \to D^- \pi^+$ and $B_s^0 \to D_s^- \pi^+$ decays, with the result of the fit superimposed. The numerical results are $q_0 = 46.1 \pm 4.1\,\text{fs}$ and $q_1 = 0.81 \pm 0.38$, with a correlation coefficient $\rho(q_0, q_1) = -0.32$. Residual small differences between signal and $B_s^0 \to D_s^- \pi^+$ decays, as seen in full simulation, are taken into account in the determination of the uncertainties on q_0 and q_1. If a simpler but less effective model based on a single Gaussian function with constant width were used, the value of such a width would have been approximately equal to 50 fs.

The distributions of δ_t for the signal components, $g_{\text{sig}}(\delta_t)$, are modelled using background-subtracted histograms. For combinatorial and three-body backgrounds, they are described using histograms obtained by studying the high- and low-mass sidebands.
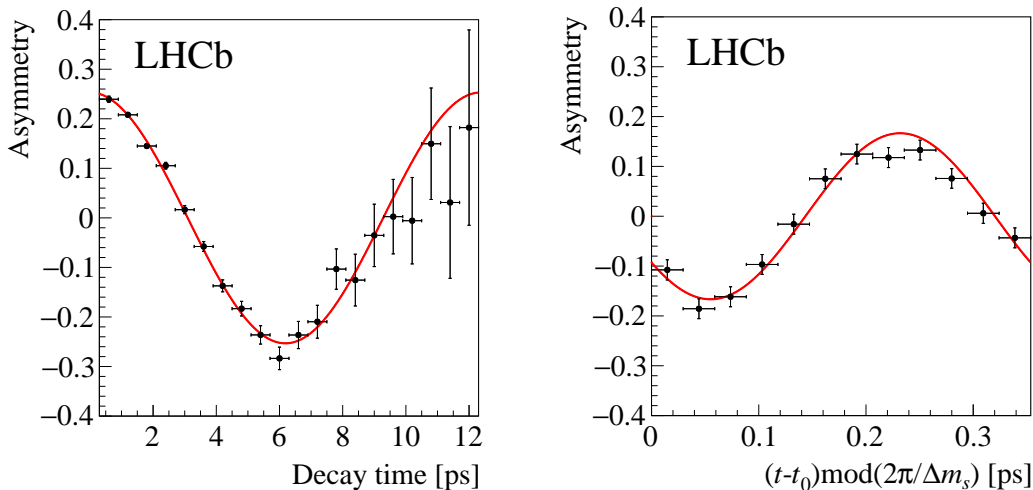
Figure 3: Time-dependent asymmetries of (left) $B^0 \to D^- \pi^+$ and (right) $B_s^0 \to D_s^- \pi^+$ decays obtained from data. The results of the best fits are superimposed. The time-dependent asymmetry of the $B_s^0 \to D_s^- \pi^+$ decays is folded into one mixing period $2\pi/\Delta m_s$ of the B_s^0 meson. The parameter $t_0 = 0.3$ ps corresponds to the minimum value allowed by the selection.

7 Detection asymmetry between $K^+\pi^-$ and $K^-\pi^+$ final states

In this section the determination of the nuisance experimental detection asymmetry, needed to determine the CP asymmetries $A_{CP}^{B^0}$ and $A_{CP}^{B_s^0}$, is described. This asymmetry arises because charge-conjugate final states are selected with different efficiencies. To excellent approximation, it can be expressed as the sum of two contributions

$$A_{\mathrm{F}} = A_{\mathrm{D}}^{K^-\pi^+} + A_{\mathrm{PID}}^{K^-\pi^+}, \tag{18}$$

where $A_{\mathrm{D}}^{K^-\pi^+}$ is the asymmetry between the efficiencies of the $K^-\pi^+$ and $K^+\pi^-$ final states without the application of the PID requirements and $A_{\mathrm{PID}}^{K^-\pi^+}$ is the asymmetry between the efficiencies of the PID requirements selecting the $K^-\pi^+$ and $K^+\pi^-$ final states.

7.1 Final-state detection asymmetry

The final-state detection asymmetry is determined using $D^+ \to K^-\pi^+\pi^+$ and $D^+ \to \overline{K}^0\pi^+$ control modes, with the neutral kaon decaying to $\pi^+\pi^-$, following the approach described in Ref. [48]. Assuming negligible CP violation in Cabibbo-favoured D-meson decays, the asymmetries between the measured yields of D^+ and D^- decays can be written as

$$A_{\mathrm{RAW}}^{K^-\pi^+\pi^+} = A_{\mathrm{P}}^{D^+} + A_{\mathrm{D}}^{K^-\pi^+} + A_{\mathrm{D}}^{\pi^+}, \tag{19}$$

$$A_{\mathrm{RAW}}^{\overline{K}^0\pi} = A_{\mathrm{P}}^{D^+} + A_{\mathrm{D}}^{\pi^+} - A_{\mathrm{D}}^{K^0}, \tag{20}$$

where $A_{\mathrm{P}}^{D^+}$ is the asymmetry between the production cross-sections of D^+ and D^- mesons, and $A_{\mathrm{D}}^{\pi^+}$ ($A_{\mathrm{D}}^{K^0}$) is the asymmetry between the detection efficiencies of π^+ (K^0) and π^-

12

$(\overline{K}^0)$ mesons. The difference between Eqs. (19) and (20) leads to

$$A_{\mathrm{D}}^{K^-\pi^+} = A_{\mathrm{RAW}}^{K^-\pi^+\pi^+} - A_{\mathrm{RAW}}^{\overline{K}^0\pi^+} - A_{\mathrm{D}}^{K^0}. \tag{21}$$

The asymmetry $A_{\mathrm{D}}^{K^0}$ was determined to be $(0.054 \pm 0.014)\,\%$ [48]. The asymmetries $A_{\mathrm{P}}^{D^+}$ and A_{D}^{π} could depend on the kinematics of the D^+ and π^+ mesons. To achieve better cancellation of these nuisance asymmetries in Eq. (21), the momentum and p_{T} of the D^+ and π^+ mesons from the $D^+ \to K^-\pi^+\pi^+$ sample are simultaneously weighted to match the corresponding distributions in the $D^+ \to \overline{K}^0\pi^+$ sample. Because of the sizeable difference in the interaction cross-sections of positive and negative kaons with the detector material, $A_{\mathrm{D}}^{K^-\pi^+}$ is determined in bins of kaon momentum. By taking into account the momentum distribution of the kaons from $B^0 \to K^+\pi^-$ and $B_s^0 \to \pi^+K^-$ decays, the values of $A_{\mathrm{D}}^{K^-\pi^+}$ for the two decay modes are found to be consistent, and the numerical result is

$$A_{\mathrm{D}}^{K^-\pi^+}\left(B^0 \to K^+\pi^-\right) = -A_{\mathrm{D}}^{K^-\pi^+}\left(B_s^0 \to \pi^+K^-\right) = (-0.91 \pm 0.14)\,\%. \tag{22}$$

The different sign of the corrections for the $B^0 \to K^+\pi^-$ and $B_s^0 \to \pi^+K^-$ decays is a consequence of the opposite definition of the final states f and $\bar{f}$ for the two modes.

7.2   Asymmetry induced by PID requirements

The PID asymmetry is determined using the calibration samples discussed in Sec. 3. Using $D^{*+} \to D^0(K^-\pi^+)\pi^+$ decays, the asymmetry between the PID efficiencies of the $K^+\pi^-$ and $K^-\pi^+$ final states is determined in bins of momentum, pseudorapidity and azimuthal angle of the two final-state particles. Several different binning schemes are used, and the average and standard deviation of the PID asymmetries determined in each scheme are used as central value and uncertainty for $A_{\mathrm{PID}}^{K^-\pi^+}$, respectively. The corrections for the two decays are found to be consistent, and the numerical result is

$$A_{\mathrm{PID}}^{K^-\pi^+}\left(B^0 \to K^+\pi^-\right) = -A_{\mathrm{PID}}^{K^-\pi^+}\left(B_s^0 \to \pi^+K^-\right) = (-0.04 \pm 0.25)\,\%. \tag{23}$$

8   Fit results

The simultaneous fit to the invariant mass, the decay time and its uncertainty, and the tagging decisions and their associated mistag probabilities for the $K^+\pi^-$, $\pi^+\pi^-$ and K^+K^- final states determines the coefficients $C_{\pi^+\pi^-}$, $S_{\pi^+\pi^-}$, $C_{K^+K^-}$, $S_{K^+K^-}$, $A_{K^+K^-}^{\Delta\Gamma}$ and the CP asymmetries $A_{CP}^{B^0}$ and $A_{CP}^{B_s^0}$. In the fits the parameters $\Delta m_{d(s)}$, $\Gamma_{d(s)}$, and $\Delta\Gamma_{d(s)}$ are fixed to the central values reported in Table 3. The signal yields are $N(B^0 \to \pi^+\pi^-) = 28\,650 \pm 230$, $N(B_s^0 \to K^+K^-) = 36\,840 \pm 220$, $N(B^0 \to K^+\pi^-) = 94\,220 \pm 340$ and $N(B_s^0 \to \pi^+K^-) = 7030 \pm 120$, where uncertainties are statistical only. The one-dimensional distributions of the measured variables used in the fit, with the results of the fit overlaid, are shown in Figs. 4, 5 and 6.

The time-dependent asymmetries, obtained separately by using the OS or the SS tagging decisions, for candidates in the region $5.20 < m < 5.32\,\mathrm{GeV}/c^2$ in the $K^+\pi^-$ spectrum, dominated by the $B^0 \to K^+\pi^-$ decay, are shown in Fig. 7. The calibration parameters of the OS and SSc taggers determined during the fit, mainly from $B^0 \to K^+\pi^-$ decays, are reported in Table 7 in App. A. The production asymmetries for the B^0 and

Table 3: Values of the parameters Δm_d, Δm_s, Γ_d, Γ_s and $\Delta\Gamma_s$ [19], fixed to their central values in the fit to the data. For Γ_s and $\Delta\Gamma_s$ the correlation factor between the two quantities is also reported. The decay width difference $\Delta\Gamma_d$ is fixed to zero.

Parameter	Value
Δm_d	$0.5065 \pm 0.0019 \, \mathrm{ps}^{-1}$
Γ_d	$0.6579 \pm 0.0017 \, \mathrm{ps}^{-1}$
$\Delta\Gamma_d$	0
Δm_s	$17.757 \pm 0.021 \ \mathrm{ps}^{-1}$
Γ_s	$0.6654 \pm 0.0022 \, \mathrm{ps}^{-1}$
$\Delta\Gamma_s$	$0.083 \pm 0.007 \ \mathrm{ps}^{-1}$
$\rho(\Gamma_s, \Delta\Gamma_s)$	-0.292

Table 4: Tagging powers for the $B^0 \to \pi^+\pi^-$ and $B_s^0 \to K^+K^-$ decays (last two rows), with a breakdown of the OS and SS contributions.

Flavour tagger	Tagging power (%)
OS	2.94 ± 0.17
SSπ	0.81 ± 0.13
SSp	0.42 ± 0.17
SSc	1.17 ± 0.11
SSK	0.71 ± 0.12
Total $B^0 \to \pi^+\pi^-$	4.08 ± 0.20
Total $B_s^0 \to K^+K^-$	3.65 ± 0.21

B_s^0 mesons are determined to be $(0.19 \pm 0.60)\%$ and $(2.4 \pm 2.1)\%$, respectively, where uncertainties are statistical only. They are consistent with the expectations from Ref. [43]. The time-dependent asymmetries for $\pi^+\pi^-$ candidates with mass values lying in the interval $5.20 < m < 5.35 \, \mathrm{GeV}/c^2$, and for K^+K^- candidates in the interval $5.30 < m < 5.45 \, \mathrm{GeV}/c^2$, both dominated by the corresponding signals, are shown in Fig. 8, again separately for the OS and SS tagging decision. The tagging powers for the $B^0 \to \pi^+\pi^-$ and $B_s^0 \to K^+K^-$ decays, together with a breakdown of the OS and SS contributions, are reported in Table 4. The results for the CP-violating quantities are

$$
\begin{aligned}
C_{\pi^+\pi^-} &= -0.34 \pm 0.06, \\
S_{\pi^+\pi^-} &= -0.63 \pm 0.05, \\
C_{K^+K^-} &= 0.20 \pm 0.06, \\
S_{K^+K^-} &= 0.18 \pm 0.06, \\
A_{K^+K^-}^{\Delta\Gamma} &= -0.79 \pm 0.07, \\
A_{CP}^{B^0} &= -0.084 \pm 0.004, \\
A_{CP}^{B_s^0} &= 0.213 \pm 0.015,
\end{aligned}
$$

where the uncertainties are statistical only and the central values of $A_{CP}^{B^0}$ and $A_{CP}^{B_s^0}$ have been

corrected for the $K^+\pi^-$ detection asymmetry. In this analysis the selection requirements and the flavour tagging performances for the various decay modes differ with respect to previous LHCb publications [17, 18]. For this reason, the statistical uncertainties are improved and do not follow a simple scaling rule with the integrated luminosity.

9   Systematic uncertainties

Two different strategies are adopted to determine systematic uncertainties on the CP-violating parameters: to account for the knowledge of external inputs whose values are fixed in the fit, the fit to the data is repeated a large number of times, each time modifying the values of these parameters; when accounting for systematic uncertainties on the fitting model, several pseudoexperiments are performed according to the baseline model, and both the baseline model and modified models are used to fit the generated data. In either case the distribution of the difference between the baseline and alternative results for the CP asymmetries is built, and the sum in quadrature of the mean and root-mean-square of the distribution is used to assign a systematic uncertainty. A detailed breakdown of the systematic uncertainties described in this Section is reported in Table 5.

The alternative models used to determine systematic uncertainties associated with the choices of the invariant-mass shapes consist in turn of: substituting the invariant-mass resolution function used for signals and cross-feed backgrounds with a single Gaussian function; fixing the parameters governing the tails of the Johnson functions and their relative amount to the same values for all signals, namely to those of the $B^0 \to K^+\pi^-$ decay; and modelling the combinatorial-background model with a linear function.

To determine a systematic uncertainty associated with the knowledge of the efficiency as a function of the decay time, $\varepsilon_{\text{sig}}(t)$, different sets of the parameters governing the efficiency functions are generated, according to their uncertainties and correlations. A systematic uncertainty associated with the choice of the decay-time model for the cross-feed backgrounds is evaluated by using an alternative model where the CP asymmetry of the $B^0 \to K^+\pi^-$ component in the $\pi^+\pi^-$ and K^+K^- final-state samples, and the C_f and S_f parameters of the $B^0 \to \pi^+\pi^-$ and $B_s^0 \to K^+K^-$ components in the $K^+\pi^-$ final-state sample, are fixed to zero. A systematic uncertainty associated with the choice of the decay-time model for the combinatorial background is evaluated using a uniform decay-time efficiency function for this component in the alternative model. A systematic uncertainty associated with the model adopted for the three-body background is evaluated by performing the fits to pseudoexperiments, removing candidates with invariant-mass values lower than $5.2\,\text{GeV}/c^2$, and removing the components describing this background from the model.

Systematic uncertainties associated with the calibration of the per-event decay-time resolution are due to the uncertainties on the parameters q_0 and q_1 and to the simulation-driven assumption that the resolution model is well described by a double Gaussian function. Different values for q_0 and q_1 are generated according to their uncertainties and correlations, and then are repeatedly used to fit the data. In addition, an alternative model for the decay-time resolution is used to assess a systematic uncertainty, including an additional contribution described by a third Gaussian function. The relative contributions of the three Gaussian functions and the ratios between their widths are determined from simulation, and the overall calibration of the new model is performed applying the same

procedure outlined in Sec. 6. A systematic uncertainty associated with the uncertainties on the parameters reported in Table 3 is determined by repeating the simultaneous fit using different fixed values, generated according to their uncertainties and correlations.

Systematic uncertainties associated with the calibration of the OS and SSc flavour-tagging responses are determined by replacing the linear relation between $\eta_{\mathrm{OS(SS)}}$ and $\omega_{\mathrm{OS(SS)}}$ of Eq. (27) with a second-order polynomial. A systematic uncertainty associated with the calibration of the SSK flavour-tagging response is determined by varying the calibration parameters reported in Table 8 according to their uncertainties and correlations. Finally, the uncertainties on the PID and detection asymmetries reported in Eqs. (23) and (22) are accounted for as systematic uncertainties on $A_{CP}^{B^0}$ and $A_{CP}^{B_s^0}$.

The total systematic uncertainties are obtained as the quadratic sum of the individual contributions, and are smaller than the corresponding statistical uncertainties for all parameters but $A_{K^+K^-}^{\Delta\Gamma}$. The dominating systematic uncertainty for $A_{K^+K^-}^{\Delta\Gamma}$ is related to the knowledge of how the efficiency varies with the decay time. Since such a dependence is determined from data, using the $B^0 \to K^+\pi^-$ decay, the size of the associated uncertainty will be reduced with future data.

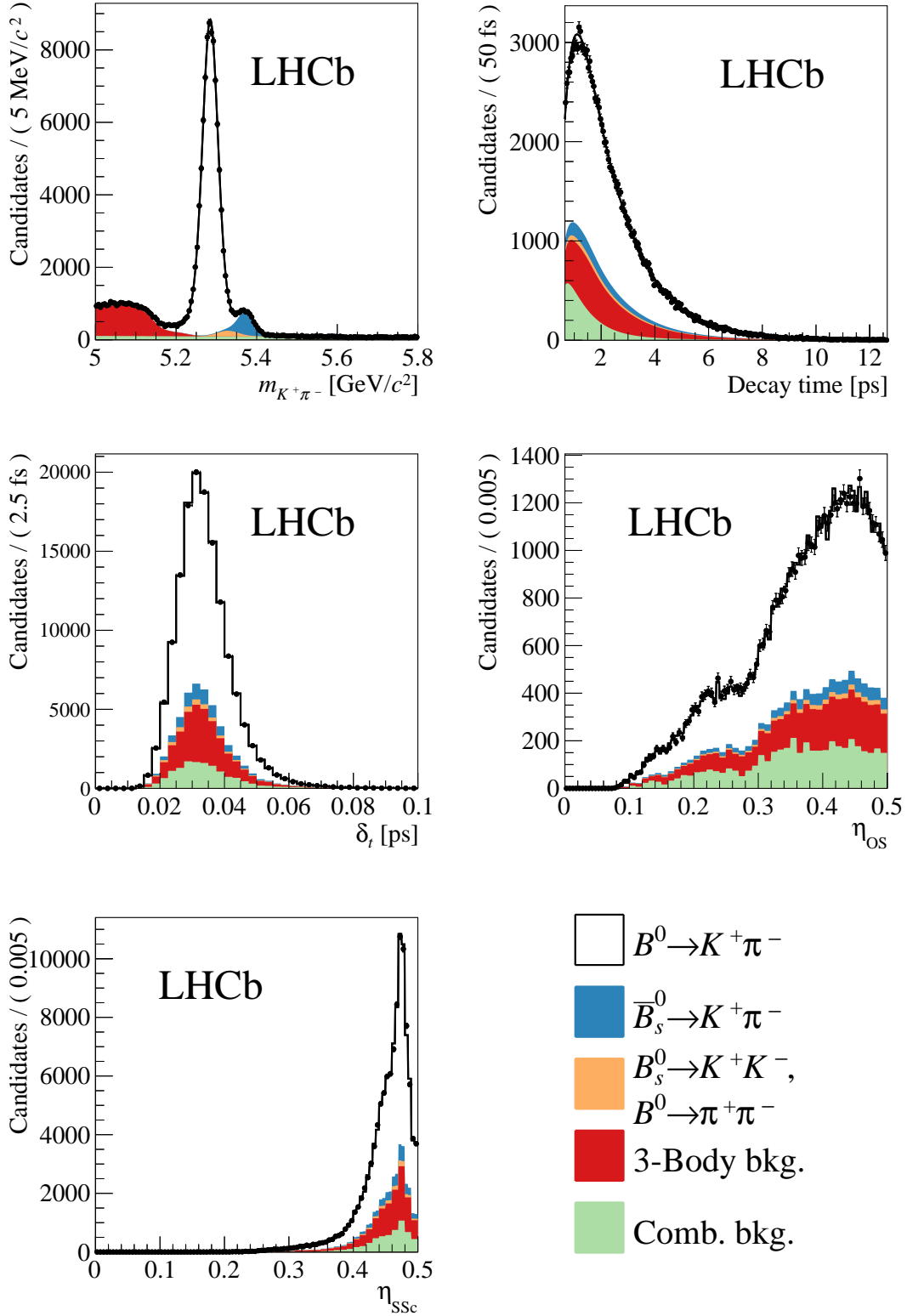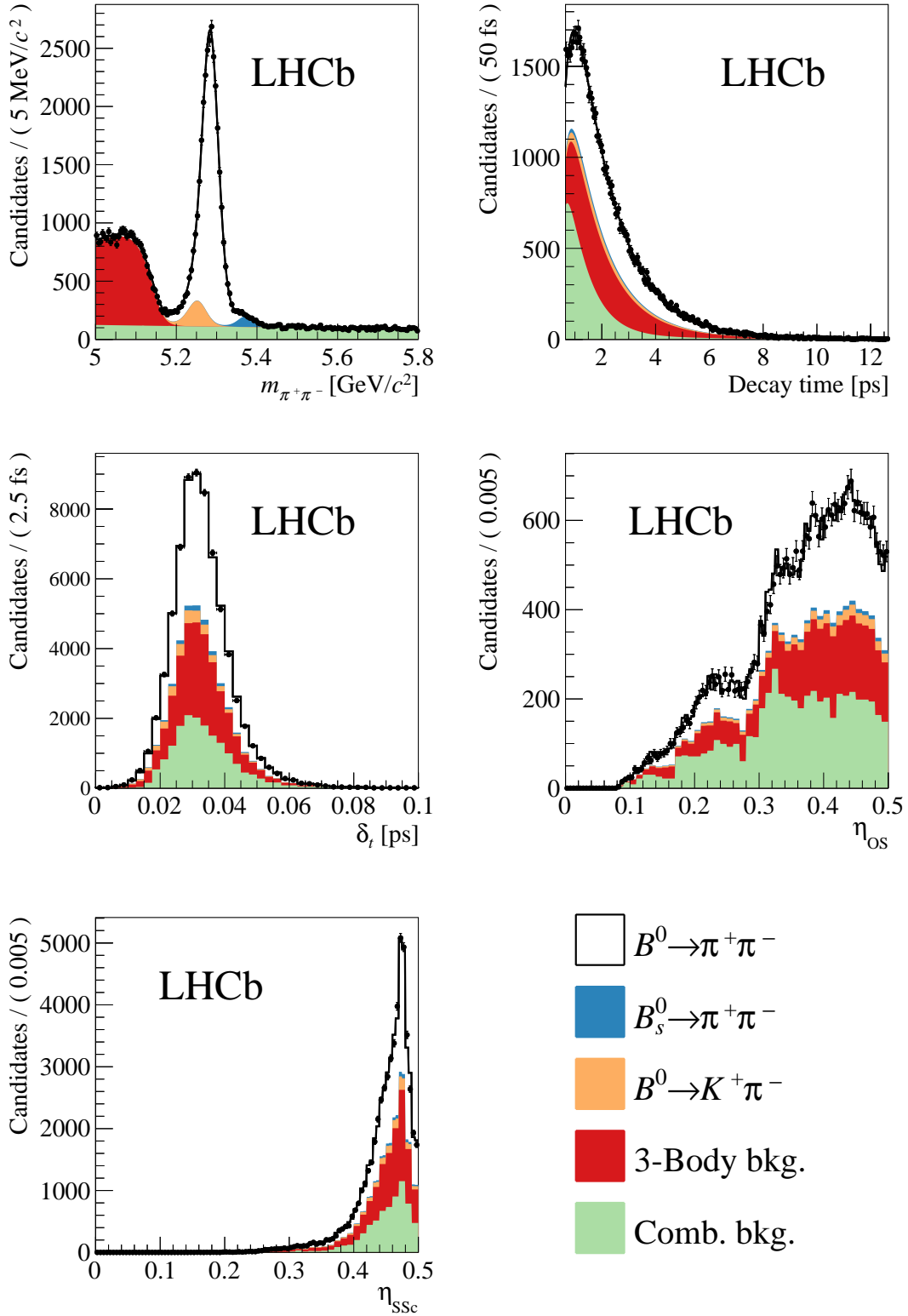Figure 4: Distributions of (top left) invariant mass, (top right) decay time, (middle left) decay-time uncertainty, (middle right) η_{OS}, and (bottom) η_{SSc} for candidates in the $K^{\pm}\pi^{\mp}$ sample. The result of the simultaneous fit is overlaid. The individual components are also shown.

Figure 5: Distributions of (top left) invariant mass, (top right) decay time, (middle left) decay-time uncertainty, (middle right) η_{OS}, and (bottom) η_{SSc} for candidates in the $\pi^+\pi^-$ sample. The result of the simultaneous fit is overlaid. The individual components are also shown.
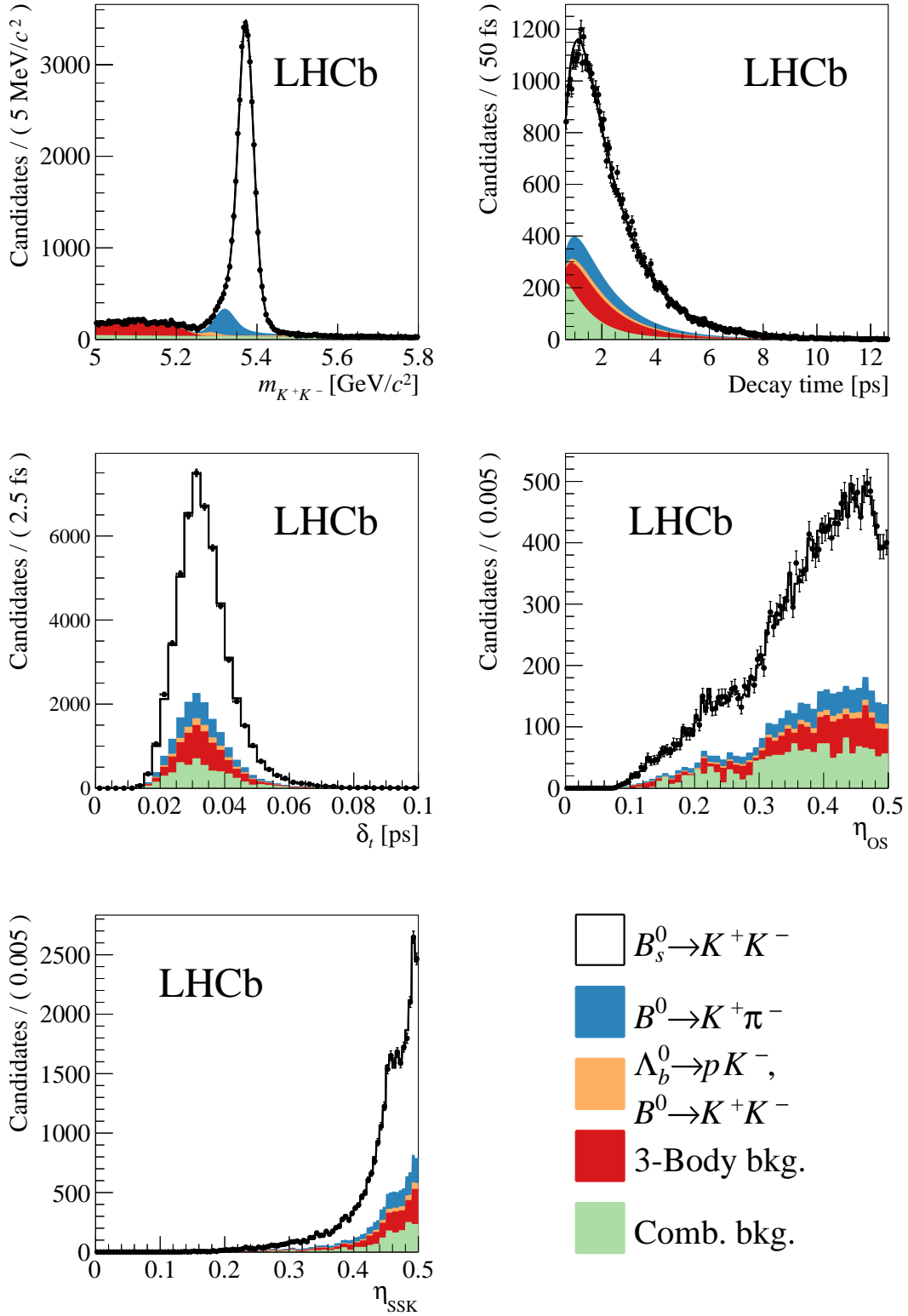
Figure 6: Distributions of (top left) invariant mass, (top right) decay time, (middle left) decay-time uncertainty, (middle right) η_{OS}, and (bottom) η_{SSK} for candidates in the K^+K^- sample. The result of the simultaneous fit is overlaid. The individual components are also shown.
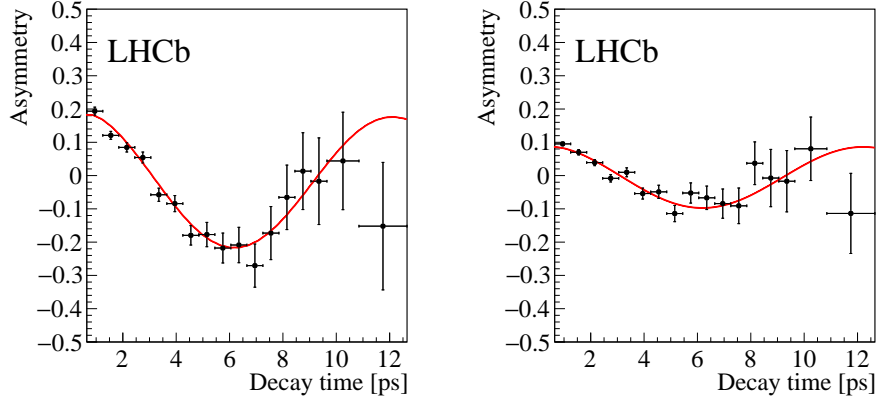
Figure 7: Time-dependent asymmetries for $K^{\pm}\pi^{\mp}$ candidates with invariant-mass values in the interval $5.20 < m < 5.32\,\mathrm{GeV}/c^2$: (left) using the OS-tagging decision and (right) the SS-tagging decision. The result of the simultaneous fit is overlaid.
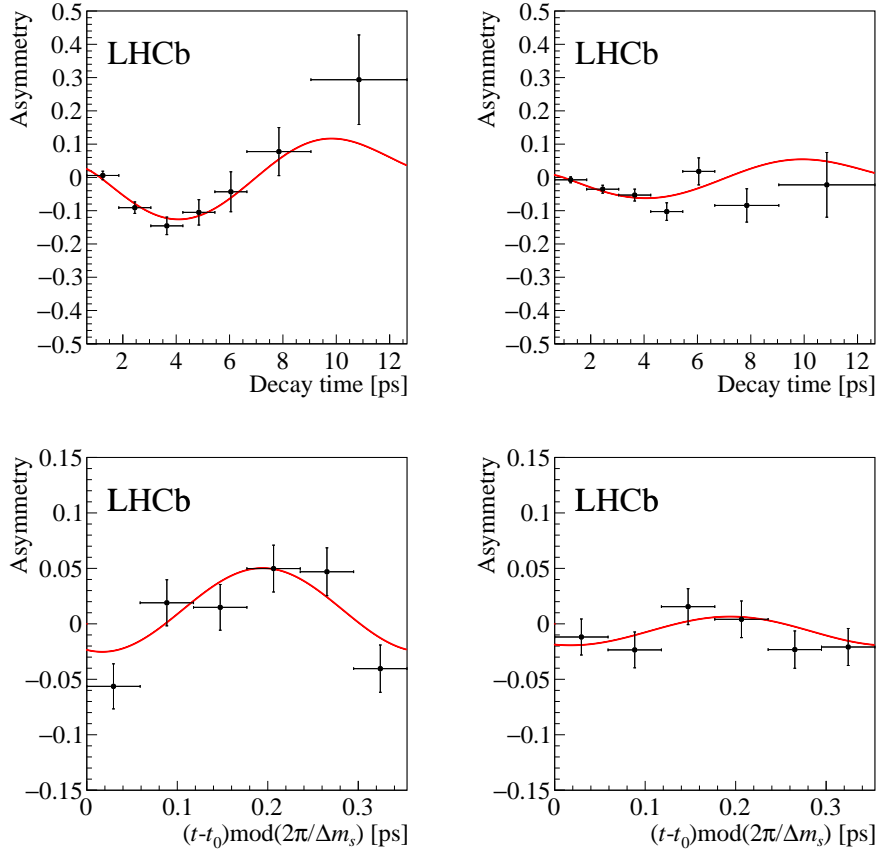

Figure 8: Time-dependent asymmetries for (top) $\pi^+\pi^-$ and (bottom) K^+K^- candidates with mass values in the intervals $5.20 < m < 5.35\,\mathrm{GeV}/c^2$ and $5.30 < m < 5.44\,\mathrm{GeV}/c^2$, respectively: (left) using the OS-tagging decision and (right) using either the SSc-tagging decision (for the $\pi^+\pi^-$ candidates) or the SSK-tagging decision (for the K^+K^- candidates). The result of the simultaneous fit is overlaid.

20

Table 5: Systematic uncertainties on the various CP-violating parameters. When present, the dash indicates that the uncertainty is not applicable to the given case.

Source of uncertainty	$C_{\pi^+\pi^-}$	$S_{\pi^+\pi^-}$	$C_{K^+K^-}$	$S_{K^+K^-}$	$A^{\Delta\Gamma}_{K^+K^-}$	$A^{B^0}_{CP}$	$A^{B^0_s}_{CP}$
Time-dependent efficiency	0.0011	0.0004	0.0020	0.0017	0.0778	0.0004	0.0002
Time-resolution calibration	0.0014	0.0013	0.0108	0.0119	0.0051	0.0001	0.0001
Time-resolution model	0.0001	0.0005	0.0002	0.0002	0.0003	negligible	negligible
Input parameters	0.0025	0.0024	0.0092	0.0107	0.0480	negligible	0.0001
OS-tagging calibration	0.0018	0.0021	0.0018	0.0019	0.0001	negligible	negligible
SSK-tagging calibration	—	—	0.0061	0.0086	0.0004	—	—
SSc-tagging calibration	0.0015	0.0017	—	—	—	negligible	negligible
Cross-feed time model	0.0075	0.0059	0.0022	0.0024	0.0003	0.0001	0.0001
Three-body bkg.	0.0070	0.0056	0.0044	0.0043	0.0304	0.0008	0.0043
Comb.-bkg. time model	0.0016	0.0016	0.0004	0.0002	0.0019	0.0001	0.0005
Signal mass model (reso.)	0.0027	0.0025	0.0015	0.0015	0.0023	0.0001	0.0041
Signal mass model (tails)	0.0007	0.0008	0.0013	0.0013	0.0016	negligible	0.0003
Comb.-bkg. mass model	0.0001	0.0003	0.0002	0.0002	0.0016	negligible	0.0001
PID asymmetry	—	—	—	—	—	0.0025	0.0025
Detection asymmetry	—	—	—	—	—	0.0014	0.0014
Total	0.0115	0.0095	0.0165	0.0191	0.0966	0.0030	0.0066

Table 6: Statistical correlations among the CP-violating parameters.

	$C_{\pi^+\pi^-}$	$S_{\pi^+\pi^-}$	$C_{K^+K^-}$	$S_{K^+K^-}$	$A^{\Delta\Gamma}_{K^+K^-}$	$A^{B^0}_{CP}$	$A^{B^0_s}_{CP}$
$C_{\pi^+\pi^-}$	1	0.448	-0.006	-0.009	0.000	-0.009	0.003
$S_{\pi^+\pi^-}$		1	-0.040	-0.006	0.000	0.008	0.000
$C_{K^+K^-}$			1	-0.014	0.025	0.006	0.001
$S_{K^+K^-}$				1	0.028	-0.003	0.000
$A^{\Delta\Gamma}_{K^+K^-}$					1	0.001	0.000
$A^{B^0}_{CP}$						1	0.043
$A^{B^0_s}_{CP}$							1

10 Conclusions

Measurements are presented of time-dependent CP violation in $B^0 \to \pi^+\pi^-$ and $B^0_s \to K^+K^-$ decays, and of the CP asymmetries in $B^0 \to K^+\pi^-$ and $B^0_s \to \pi^+K^-$ decays, based on a data sample of pp collisions corresponding to an integrated luminosity of $3.0\,\text{fb}^{-1}$ collected with the LHCb detector at centre-of-mass energies of 7 and 8 TeV. The results are

$$
\begin{aligned}
C_{\pi^+\pi^-} &= -0.34 \pm 0.06 \pm 0.01, \\
S_{\pi^+\pi^-} &= -0.63 \pm 0.05 \pm 0.01, \\
C_{K^+K^-} &= 0.20 \pm 0.06 \pm 0.02, \\
S_{K^+K^-} &= 0.18 \pm 0.06 \pm 0.02, \\
A^{\Delta\Gamma}_{K^+K^-} &= -0.79 \pm 0.07 \pm 0.10, \\
A^{B^0}_{CP} &= -0.084 \pm 0.004 \pm 0.003, \\
A^{B^0_s}_{CP} &= 0.213 \pm 0.015 \pm 0.007,
\end{aligned}
$$

where the first uncertainties are statistical and the second systematic. They supersede with much improved precision those of Refs. [17, 18]. The corresponding statistical correlation matrix is reported in Table 6. Taking into account the sizes of statistical and systematic uncertainties, correlations due to the latter can be neglected. The measurements of $C_{\pi^+\pi^-}$, $S_{\pi^+\pi^-}$, $A^{B^0}_{CP}$ and $A^{B^0_s}_{CP}$ are the most precise from a single experiment to date, and are in good agreement with previous determinations [22–25]. Those of $C_{K^+K^-}$ and $S_{K^+K^-}$ are in good agreement with the previous LHCb result [17]. By summing in quadrature the statistical and systematic uncertainties and neglecting the small correlations between $C_{K^+K^-}$, $S_{K^+K^-}$ and $A^{\Delta\Gamma}_{K^+K^-}$, the significance for $(C_{K^+K^-}, S_{K^+K^-}, A^{\Delta\Gamma}_{K^+K^-})$ to differ from $(0, 0, -1)$ is determined by means of a χ^2 test statistic to be 4.0 standard deviations. This result constitutes the strongest evidence for time-dependent CP violation in the B^0_s-meson sector to date. As a cross-check, the distribution of the variable Q, defined by $Q^2 = (C_{K^+K^-})^2 + (S_{K^+K^-})^2 + (A^{\Delta\Gamma}_{K^+K^-})^2$, is studied by generating, according to the multivariate Gaussian function defined by their uncertainties and correlations, a large sample of values for the variables $C_{K^+K^-}$, $S_{K^+K^-}$ and $A^{\Delta\Gamma}_{K^+K^-}$. The distribution of Q is found to be Gaussian, with mean 0.83 and width 0.12.

The measurements of $A_{CP}^{B^0}$ and $A_{CP}^{B_s^0}$ allow a test of the validity of the SM, as suggested in Ref. [7], by checking the equality

$$\Delta = \frac{A_{CP}^{B^0}}{A_{CP}^{B_s^0}} + \frac{\mathcal{B}\left(B_s^0 \to \pi^+K^-\right)}{\mathcal{B}\left(B^0 \to K^+\pi^-\right)} \frac{\tau_d}{\tau_s} = 0, \tag{24}$$

where $\mathcal{B}\left(B^0 \to K^+\pi^-\right)$ and $\mathcal{B}\left(B_s^0 \to \pi^+K^-\right)$ are CP-averaged branching fractions, and τ_d and τ_s are the B^0 and B_s^0 mean lifetimes, respectively. Using the world averages for $f_s/f_d \times \mathcal{B}\left(B_s^0 \to \pi^+K^-\right)/\mathcal{B}\left(B^0 \to K^+\pi^-\right)$ and τ_s/τ_d [19] and the measurement of the relative hadronisation fraction between B_s^0 and B^0 mesons $f_s/f_d = 0.259 \pm 0.015$ [49], the value $\Delta = -0.11 \pm 0.04 \pm 0.03$ is obtained, where the first uncertainty is from the measurements of the CP asymmetries and the second is from the input values of the branching fractions, the lifetimes and the hadronisation fractions. No evidence for a deviation from zero of Δ is observed with the present experimental precision.

These new measurements will enable improved constraints to be set on the CKM CP-violating phases, using processes whose amplitudes receive significant contributions from loop diagrams both in the mixing and decay of $B_{(s)}^0$ mesons [9–11]. Comparisons with tree-level determinations of the same phases will provide tests of the SM and constrain possible new-physics contributions.

Acknowledgements

Appendix

A   Flavour-tagging details

A.1   Formalism

The functions $\Omega_{\text{sig}}(\vec{\xi}, \vec{\eta})$ and $\bar{\Omega}_{\text{sig}}(\vec{\xi}, \vec{\eta})$ in Eqs. (8) and (11) are

$$
\begin{aligned}
\Omega_{\text{sig}}(\vec{\xi}, \vec{\eta}) &= \Omega_{\text{sig}}^{\text{OS}}(\xi_{\text{OS}}, \eta_{\text{OS}})\, \Omega_{\text{sig}}^{\text{SS}}(\xi_{\text{SS}}, \eta_{\text{SS}}), \\
\bar{\Omega}_{\text{sig}}(\vec{\xi}, \vec{\eta}) &= \bar{\Omega}_{\text{sig}}^{\text{OS}}(\xi_{\text{OS}}, \eta_{\text{OS}})\, \bar{\Omega}_{\text{sig}}^{\text{SS}}(\xi_{\text{SS}}, \eta_{\text{SS}}),
\end{aligned}
\tag{25}
$$

where $\Omega_{\text{sig}}^{\text{tag}}(\xi_{\text{tag}}, \eta_{\text{tag}})$ and $\bar{\Omega}_{\text{sig}}^{\text{tag}}(\xi_{\text{tag}}, \eta_{\text{tag}})$ (with tag $\in \{$OS, SS$\}$) are

$$
\begin{aligned}
\Omega_{\text{sig}}^{\text{tag}}(\xi_{\text{tag}}, \eta_{\text{tag}}) =\, & \delta_{\xi_{\text{tag}}, 1}\, \varepsilon_{\text{sig}}^{\text{tag}}\, [1 - \omega_{\text{tag}}(\eta_{\text{tag}})]\, h_{\text{sig}}^{\text{tag}}(\eta_{\text{tag}}) + \\
& \delta_{\xi_{\text{tag}}, -1}\, \varepsilon_{\text{sig}}^{\text{tag}}\, \omega_{\text{tag}}(\eta_{\text{tag}})\, h_{\text{sig}}^{\text{tag}}(\eta_{\text{tag}}) + \\
& \delta_{\xi_{\text{tag}}, 0}\, (1 - \varepsilon_{\text{sig}}^{\text{tag}})\, U(\eta_{\text{tag}}), \\
\bar{\Omega}_{\text{sig}}^{\text{tag}}(\xi_{\text{tag}}, \eta_{\text{tag}}) =\, & \delta_{\xi_{\text{tag}}, -1}\, \bar{\varepsilon}_{\text{sig}}^{\text{tag}}\, [1 - \bar{\omega}_{\text{tag}}(\eta_{\text{tag}})]\, h_{\text{sig}}^{\text{tag}}(\eta_{\text{tag}}) + \\
& \delta_{\xi_{\text{tag}}, 1}\, \bar{\varepsilon}_{\text{sig}}^{\text{tag}}\, \bar{\omega}_{\text{tag}}(\eta_{\text{tag}})\, h_{\text{sig}}^{\text{tag}}(\eta_{\text{tag}}) + \\
& \delta_{\xi_{\text{tag}}, 0}\, (1 - \bar{\varepsilon}_{\text{sig}}^{\text{tag}})\, U(\eta_{\text{tag}}).
\end{aligned}
\tag{26}
$$

The symbol $\delta_{\xi_{\text{tag}}, i}$ stands for the Kronecker delta function, $\varepsilon_{\text{sig}}^{\text{tag}}$ ($\bar{\varepsilon}_{\text{sig}}^{\text{tag}}$) is the probability that the flavour of a $B_{(s)}^0$ ($\bar{B}_{(s)}^0$) meson is tagged, $\omega_{\text{tag}}(\eta_{\text{tag}})$ ($\bar{\omega}_{\text{tag}}(\eta_{\text{tag}})$) is the calibrated mistag probability as a function of η_{tag} for a $B_{(s)}^0$ ($\bar{B}_{(s)}^0$) meson, $h_{\text{sig}}^{\text{tag}}(\eta_{\text{tag}})$ is the PDF describing the distribution of η_{tag} for tagged events, and $U(\eta_{\text{tag}})$ is a uniform distribution of η_{tag}. It is empirically found that, to a good approximation, η_{tag} and ω_{tag} are related by a linear function, *i.e.*

$$
\begin{aligned}
\omega_{\text{tag}}(\eta_{\text{tag}}) &= p_0^{\text{tag}} + p_1^{\text{tag}}\, (\eta_{\text{tag}} - \hat{\eta}_{\text{tag}}), \\
\bar{\omega}_{\text{tag}}(\eta_{\text{tag}}) &= \bar{p}_0^{\text{tag}} + \bar{p}_1^{\text{tag}}\, (\eta_{\text{tag}} - \hat{\eta}_{\text{tag}}),
\end{aligned}
\tag{27}
$$

where $\hat{\eta}_{\text{tag}}$ is a fixed value, chosen to be equal to the mean value of the η_{tag} distribution to minimise the correlation among the parameters. To reduce the correlation among $\varepsilon_{\text{sig}}^{\text{tag}}$ and $\bar{\varepsilon}_{\text{sig}}^{\text{tag}}$, and p_0^{tag}, $\bar{p}_0^{\text{tag}}$, p_1^{tag}, and $\bar{p}_1^{\text{tag}}$, these variables are conveniently parameterised as

$$
\begin{aligned}
\varepsilon_{\text{sig}}^{\text{tag}} &= \hat{\varepsilon}_{\text{sig}}^{\text{tag}}(1 + \Delta\varepsilon_{\text{sig}}^{\text{tag}}), \\
\bar{\varepsilon}_{\text{sig}}^{\text{tag}} &= \hat{\varepsilon}_{\text{sig}}^{\text{tag}}(1 - \Delta\varepsilon_{\text{sig}}^{\text{tag}}), \\
p_0^{\text{tag}} &= \hat{p}_0^{\text{tag}}(1 + \Delta p_0^{\text{tag}}), \\
\bar{p}_0^{\text{tag}} &= \hat{p}_0^{\text{tag}}(1 - \Delta p_0^{\text{tag}}), \\
p_1^{\text{tag}} &= \hat{p}_1^{\text{tag}}(1 + \Delta p_1^{\text{tag}}), \\
\bar{p}_1^{\text{tag}} &= \hat{p}_1^{\text{tag}}(1 - \Delta p_1^{\text{tag}}),
\end{aligned}
\tag{28}
$$

where $\hat{p}_{0,1}^{\text{tag}}$ and $\Delta p_{0,1}^{\text{tag}}$ are the average and the asymmetry between $p_{0,1}^{\text{tag}}$ and $\bar{p}_{0,1}^{\text{tag}}$, and $\hat{\varepsilon}_{\text{sig}}^{\text{tag}}$ and $\Delta\varepsilon_{\text{sig}}^{\text{tag}}$ are the average and the asymmetry between $\varepsilon_{\text{sig}}^{\text{tag}}$ and $\bar{\varepsilon}_{\text{sig}}^{\text{tag}}$. The PDF $h_{\text{sig}}^{\text{OS}}(\eta)$ is

modelled using background-subtracted histograms of signal candidates. The description of $h_{\text{sig}}^{\text{SS}}(\eta)$ for the SS taggers is presented in Secs. A.2 and A.3, respectively.

The PDF of ξ_{tag} and η_{tag} for the combinatorial background is empirically parameterised as

$$
\Omega_{\text{comb}}^{\text{tag}}(\xi_{\text{tag}},\,\eta_{\text{tag}}) = \delta_{\xi_{\text{tag}},\,1}\varepsilon_{\text{comb}}^{\text{tag}}\,h_{\text{comb}}^{\text{tag}}(\eta_{\text{tag}}) \,+\, \delta_{\xi_{\text{tag}},\,-1}\bar{\varepsilon}_{\text{comb}}^{\text{tag}}\,h_{\text{comb}}^{\text{tag}}(\eta_{\text{tag}}) +
$$
$$
\delta_{\xi_{\text{tag}},\,0}\,(1 - \varepsilon_{\text{comb}}^{\text{tag}} - \bar{\varepsilon}_{\text{comb}}^{\text{tag}})\,U(\eta_{\text{tag}}),
\tag{29}
$$

where $\varepsilon_{\text{comb}}^{\text{tag}}$ and $\bar{\varepsilon}_{\text{comb}}^{\text{tag}}$ are the efficiencies to tag a combinatorial-background candidate as $B_{(s)}^0$ or $\overline{B}_{(s)}^0$, respectively, $h_{\text{comb}}^{\text{tag}}(\eta_{\text{tag}})$ is the PDF of η_{tag}. As done for the signal model, the tagging efficiencies are parameterised as

$$
\varepsilon_{\text{comb}}^{\text{tag}} \;=\; \frac{\hat{\varepsilon}_{\text{comb}}^{\text{tag}}}{2}(1 + \Delta\varepsilon_{\text{comb}}^{\text{tag}}),
\tag{30}
$$
$$
\bar{\varepsilon}_{\text{comb}}^{\text{tag}} \;=\; \frac{\hat{\varepsilon}_{\text{comb}}^{\text{tag}}}{2}(1 - \Delta\varepsilon_{\text{comb}}^{\text{tag}}),
$$

such that the fits determine the total efficiency to tag a combinatorial-background candidate as $B_{(s)}^0$ or $\overline{B}_{(s)}^0$ ($\hat{\varepsilon}_{\text{comb}}^{\text{tag}}$), and the asymmetry between the two efficiencies ($\Delta\varepsilon_{\text{comb}}^{\text{tag}}$). The PDF $h_{\text{comb}}^{\text{tag}}(\eta_{\text{tag}})$ is determined as a histogram from the high-mass sideband where only combinatorial background is present. The combined PDF of ξ_{OS}, ξ_{SS}, η_{OS} and η_{SS}, analogously to the signal case, is given by

$$
\Omega_{\text{comb}}(\vec{\xi},\,\vec{\eta}) = \Omega_{\text{comb}}^{\text{OS}}(\xi_{\text{OS}},\,\eta_{\text{OS}}) \cdot \Omega_{\text{comb}}^{\text{SS}}(\xi_{\text{SS}},\,\eta_{\text{SS}}).
\tag{31}
$$

The PDF of ξ_{tag} and η_{tag} for three-body backgrounds in the $\pi^+\pi^-$ and K^+K^- spectra is empirically parameterised as

$$
\Omega_{\text{3-body}}^{\text{tag}}(\xi_{\text{tag}},\,\eta_{\text{tag}}) = \delta_{\xi_{\text{tag}},\,1}\varepsilon_{\text{3-body}}^{\text{tag}}\,h_{\text{3-body}}^{\text{tag}}(\eta_{\text{tag}}) \,+\, \delta_{\xi_{\text{tag}},\,-1}\bar{\varepsilon}_{\text{3-body}}^{\text{tag}}\,h_{\text{3-body}}^{\text{tag}}(\eta_{\text{tag}}) +
$$
$$
\delta_{\xi_{\text{tag}},\,0}\,(1 - \varepsilon_{\text{3-body}}^{\text{tag}} - \bar{\varepsilon}_{\text{3-body}}^{\text{tag}})\,U(\eta_{\text{tag}}),
\tag{32}
$$

where $\varepsilon_{\text{3-body}}^{\text{tag}}$ and $\bar{\varepsilon}_{\text{3-body}}^{\text{tag}}$ are the efficiencies to tag a background candidate as $B_{(s)}^0$ or $\overline{B}_{(s)}^0$, respectively, and $h_{\text{3-body}}^{\text{tag}}(\eta_{\text{tag}})$ is the PDF of η_{tag}. Also in this case the tagging efficiencies are parameterised as a function of the total efficiency ($\hat{\varepsilon}_{\text{3-body}}^{\text{tag}}$) and asymmetry ($\Delta\varepsilon_{\text{3-body}}^{\text{tag}}$)

$$
\varepsilon_{\text{3-body}}^{\text{tag}} \;=\; \frac{\hat{\varepsilon}_{\text{3-body}}^{\text{tag}}}{2}(1 + \Delta\varepsilon_{\text{3-body}}^{\text{tag}}),
\tag{33}
$$
$$
\bar{\varepsilon}_{\text{3-body}}^{\text{tag}} \;=\; \frac{\hat{\varepsilon}_{\text{3-body}}^{\text{tag}}}{2}(1 - \Delta\varepsilon_{\text{3-body}}^{\text{tag}}).
$$

The PDF $h_{\text{3-body}}^{\text{tag}}(\eta_{\text{tag}})$ is determined as a histogram from the low-mass sideband, where the residual contamination of combinatorial-background candidates is subtracted. As mentioned in Sec. 4.2, for the $K^+\pi^-$ final-state sample the three-body background is parameterised in the same way as for the $B^0 \to K^+\pi^-$ decay, but with independent parameters for the flavour-tagging calibration.

The PDFs in Eqs. (25), (31) and (32) are valid if η_{OS} and η_{SS} are uncorrelated variables. This assumption is verified by means of background-subtracted [50] signals, and of candidates from the high- and low-mass sidebands for the combinatorial and three-body backgrounds, respectively.
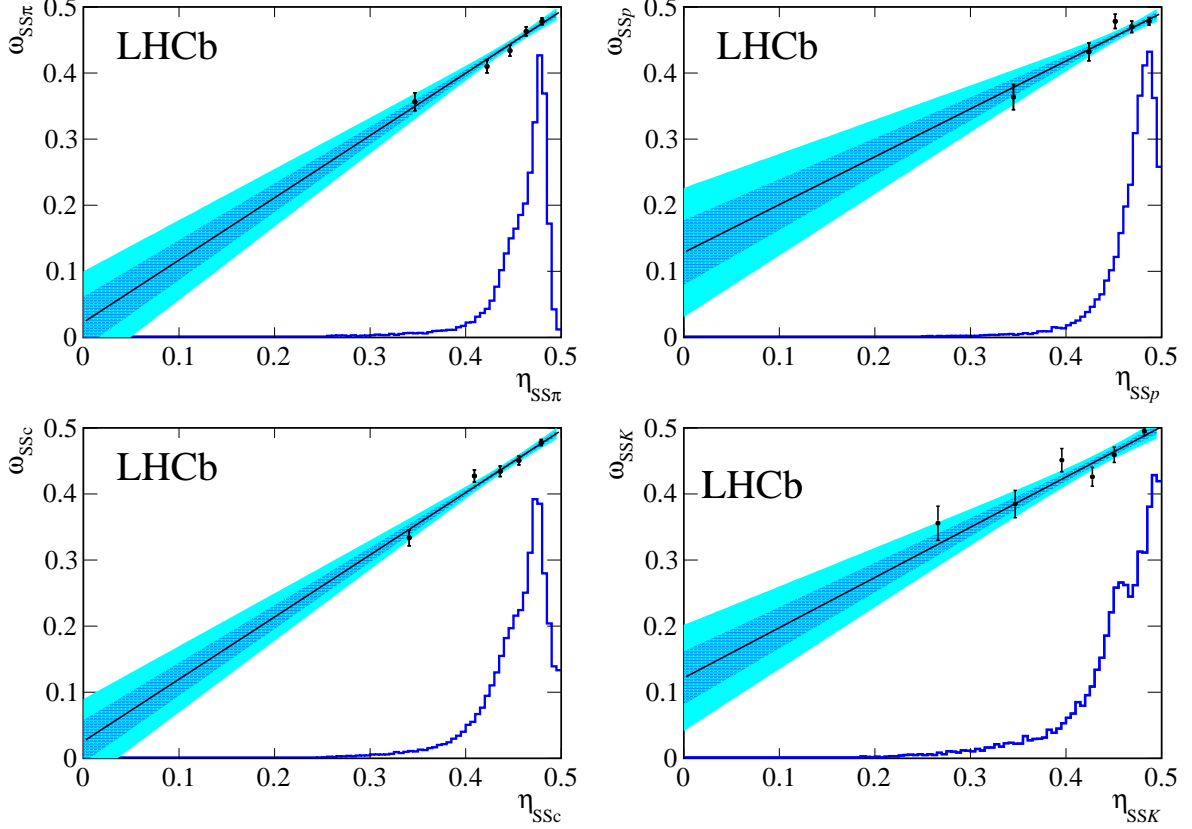
Figure 9: Relation between ω_{tag} on η_{tag} for (top left) SSπ, (top right) SSp, (bottom left) SSc and (bottom right) SSK taggers. The black dots represent the average value of ω_{tag} in bins of η_{tag}, as described in the text. The black straight line represents the linear relation between ω_{tag} and η_{tag} obtained from the calibration procedure. The darker and brighter areas are the corresponding 68% and 95% confidence intervals, respectively. The distributions of η_{tag} are also reported as histograms with arbitrary normalisations.

A.2 Combination of the SSπ and SSp taggers

The SSπ and SSp taggers are calibrated separately using background-subtracted $B^0 \to K^+\pi^-$ decays. By using the PDF in Eq. (8) to perform a fit to the tagged decay-time distribution of these candidates, the parameters governing the relations in Eqs. (25) are determined separately for the two taggers. The calibration parameters determined from the fit are used to combine the two taggers into a unique one (SSc) with decision ξ_{SSc} and mistag probability η_{SSc}. To validate the assumption of a linear relation between η_{tag} and ω_{tag}, the sample is split into bins of $\eta_{SS\pi(SSp)}$, such that each subsample has approximately the same tagging power. The average mistag fraction in each bin is determined by means of a tagged time-dependent fit to the various subsamples. This check is performed separately for the SSπ, SSp and SSc. The results of the calibration procedure and of the cross-check using the fits in bins of $\eta_{SS\pi}$, η_{SSp} and η_{SSc} are shown in Fig. 9. The final calibration for η_{SSc} is performed during the final fit, and the values of the calibration parameters are reported later in Table 7.

The PDFs $h_{sig}^{SS}(\eta_{SSc})$ describing the η_{SSc} distributions for the signal B^0 mesons are de-

Table 7: Values for the calibration parameters of the flavour tagging obtained from the fits. The values of $\hat{\eta}_{\mathrm{OS}}$ and $\hat{\eta}_{\mathrm{SS}}$ are fixed in the fit to 0.37 and 0.44, respectively.

Parameter	Value
$\hat{p}_0^{\mathrm{OS}}$	0.385 ± 0.004
Δp_0^{OS}	0.016 ± 0.006
$\hat{p}_1^{\mathrm{OS}}$	$1.02 \ \pm 0.04$
Δp_1^{OS}	0.029 ± 0.024
$\hat{p}_0^{\mathrm{SSc}}$	0.438 ± 0.003
$\Delta p_0^{\mathrm{SSc}}$	0.002 ± 0.004
$\hat{p}_1^{\mathrm{SSc}}$	$0.96 \ \pm 0.07$
$\Delta p_1^{\mathrm{SSc}}$	$-0.03 \ \pm 0.04$

termined using background-subtracted histograms of $B^0 \to D^- \pi^+$ decays. It is empirically found that the distribution of η_{SSc} has a sizeable dependence on the B^0-meson p_{T}. Hence the $B^0 \to D^- \pi^+$ sample is weighted in order to equalise the p_{T} distribution to that of the signal.

A.3 Calibration of the SSK tagger

To calibrate the response of the SSK tagger, the natural control mode would be the $B_s^0 \to \pi^+ K^-$ decay. However, the signal yield of this decay is approximately 8% of that of the $B^0 \to K^+ \pi^-$ decay, and 20% of that of the $B_s^0 \to K^+ K^-$ decay. Hence the calibration parameters of the SSK tagger would be affected by large uncertainties, limiting the precision on $C_{K^+ K^-}$ and $S_{K^+ K^-}$. Therefore, the calibration is performed with a large sample of $B_s^0 \to D_s^- \pi^+$ decays. Analogously to the SSπ and SSp cases, the SSK-calibration parameters are determined using an unbinned maximum likelihood fit to the tagged decay-time distribution of the $B_s^0 \to D_s^- \pi^+$ decay. The PDF used to fit the decay-time rate is the same as that for the SSπ and SSp taggers. The fit is performed using the flavour-tagging information on a per-event basis, determining the calibration parameters directly. To check the linearity of the relation between $\eta_{\mathrm{SS}K}$ and $\omega_{\mathrm{SS}K}$, the sample is again divided in bins of $\eta_{\mathrm{SS}K}$ and the average $\omega_{\mathrm{SS}K}$ is determined in each bin (see Fig. 9).

The SSK tagger uses kaons coming from the hadronisation of the beauty quark to determine the flavour of the B_s^0 meson. As the kaon kinematics are correlated to those of the B_s^0 meson, the performance of the SSK tagger also depends on the latter. To take into account the differences between the B_s^0-meson kinematics and other relevant distributions in $B_s^0 \to D_s^- \pi^+$ and $B_s^0 \to K^+ K^-$ decays, due to the different topologies and selection requirements, a weighting procedure is applied to the $B_s^0 \to D_s^- \pi^+$ sample. It is empirically found that the distributions of the following variables need to be equalised: the transverse momentum, the pseudorapidity and the azimuthal angle of the B_s^0 meson, and the number of PVs and tracks in the events. The results of the fit to the weighted sample are reported in Table 8.

The PDF $h_{\mathrm{sig}}^{\mathrm{SS}K}(\eta_{\mathrm{SS}K})$ for $B_s^0 \to K^+ K^-$ decays is determined using a background-

Table 8: Calibration parameters for the SSK tagger.

Parameter	Value
$\hat{p}_0^{\mathrm{SSK}}$	0.456 ± 0.005
$\Delta p_0^{\mathrm{SSK}}$	-0.011 ± 0.005
$\hat{p}_1^{\mathrm{SSK}}$	$0.76 \ \pm 0.09$
$\Delta p_1^{\mathrm{SSK}}$	$0.03 \ \pm 0.05$

subtracted histogram of the same weighted sample of $B_s^0 \to D_s^- \pi^+$ decays used for the calibration.

References

[1] N. Cabibbo, *Unitary Symmetry and Leptonic Decays*, Phys. Rev. Lett. **10** (1963) 531.

[2] M. Kobayashi and T. Maskawa, *CP Violation in the Renormalizable Theory of Weak Interaction*, Prog. Theor. Phys. **49** (1973) 652.

[3] N. G. Deshpande and X.-G. He, *CP asymmetry relations between $\overline{B}^0 \to \pi\pi$ and $\overline{B}^0 \to \pi K$ rates*, Phys. Rev. Lett. **75** (1995) 1703, `arXiv:hep-ph/9412393`.

[4] X.-G. He, *SU(3) analysis of annihilation contributions and CP violating relations in $B \to PP$ decays*, Eur. Phys. J. **C9** (1999) 443, `arXiv:hep-ph/9810397`.

[5] R. Fleischer, *New strategies to extract β and γ from $B_d \to \pi^+\pi^-$ and $B_s \to K^+K^-$*, Phys. Lett. **B459** (1999) 306, `arXiv:hep-ph/9903456`.

[6] M. Gronau and J. L. Rosner, *The role of $B_s^0 \to \pi K$ in determining the weak phase γ*, Phys. Lett. **B482** (2000) 71, `arXiv:hep-ph/0003119`.

[7] H. J. Lipkin, *Is observed direct CP violation in $B^0 \to K^+\pi^-$ due to new physics? Check standard model prediction of equal violation in $B_s^0 \to K^-\pi^+$*, Phys. Lett. **B621** (2005) 126, `arXiv:hep-ph/0503022`.

[8] R. Fleischer, *$B_{s,d} \to \pi\pi, \pi K, KK$: status and prospects*, Eur. Phys. J. **C52** (2007) 267, `arXiv:0705.1121`.

[9] R. Fleischer and R. Kneigjens, *In pursuit of new physics with $B_s^0 \to K^+K^-$*, Eur. Phys. J. **C71** (2011) 1, `arXiv:1011.1096`.

[10] M. Ciuchini *et al.*, *Testing the standard model and searching for new physics with $B^0 \to \pi^+\pi^-$ and $B_s^0 \to K^+K^-$ decays*, JHEP **10** (2012) 29, `arXiv:1205.4948`.

[11] LHCb collaboration, R. Aaij *et al.*, *Determination of γ and $-2\beta_s$ from charmless two-body decays of beauty mesons*, Phys. Lett. **B739** (2015) 1, `arXiv:1408.4368`.

[12] R. Fleischer, R. Jaarsma, and K. K. Vos, *New strategy to explore CP violation with $B_s^0 \to K^+K^-$*, Phys. Rev. **D94** (2016) 113014, `arXiv:1608.00901`.

[13] R. Fleischer, R. Jaarsma, and K. K. Vos, *Towards new frontiers in the exploration of charmless non-leptonic B decays*, JHEP **03** (2017) 055, arXiv:1612.07342.

[14] M. Gronau and D. London, *Isospin analysis of CP asymmetries in B decays*, Phys. Rev. Lett. **65** (1990) 3381.

[15] UTfit collaboration, M. Bona *et al.*, *Improved determination of the CKM angle α from $B \to \pi\pi$ decays*, Phys. Rev. D **76** (2007) 014015, arXiv:hep-ph/0701204.

[16] J. Charles, O. Deschamps, S. Descotes-Genon, and V. Niess, *Isospin analysis of charmless B-meson decays*, Eur. Phys. J. **C77** (2017) 574, arXiv:1705.02981.

[17] LHCb collaboration, R. Aaij *et al.*, *First measurement of time-dependent CP violation in $B_s^0 \to K^+K^-$ decays*, JHEP **10** (2013) 183, arXiv:1308.1428.

[18] LHCb collaboration, R. Aaij *et al.*, *First observation of CP violation in the decays of B_s^0 mesons*, Phys. Rev. Lett. **110** (2013) 221601, arXiv:1304.6173.

[19] Heavy Flavor Averaging Group, Y. Amhis *et al.*, *Averages of b-hadron, c-hadron, and τ-lepton properties as of summer 2016*, Eur. Phys. J. **C77** (2017) 895, arXiv:1612.07233, updated results and plots available at https://hflav.web.cern.ch.

[20] LHCb collaboration, R. Aaij *et al.*, *Measurement of the CP asymmetry in B_s^0–$\overline{B}_s^0$ mixing*, Phys. Rev. Lett. **117** (2016) 061803, arXiv:1605.09768.

[21] LHCb collaboration, R. Aaij *et al.*, *Measurement of the semileptonic CP asymmetry in B^0–$\overline{B}^0$ mixing*, Phys. Rev. Lett. **114** (2015) 041601, arXiv:1409.8586.

[22] BaBar collaboration, J. P. Lees *et al.*, *Measurement of CP asymmetries and branching fractions in charmless two-body B-meson decays to pions and kaons*, Phys. Rev. **D87** (2013) 052009, arXiv:1206.3525.

[23] Belle collaboration, J. Dalseno *et al.*, *Measurement of the CP violation parameters in $B^0 \to \pi^+\pi^-$ decays*, Phys. Rev. **D88** (2013) 092003, arXiv:1302.0551.

[24] Belle collaboration, Y.-T. Duh *et al.*, *Measurements of branching fractions and direct CP asymmetries for $B \to K\pi$, $B \to \pi\pi$ and $B \to KK$ decays*, Phys. Rev. **D87** (2013) 031103, arXiv:1210.1348.

[25] CDF collaboration, T. A. Aaltonen *et al.*, *Measurements of direct CP-violating asymmetries in charmless decays of bottom baryons*, Phys. Rev. Lett. **113** (2014) 242001, arXiv:1403.5586.

[26] LHCb collaboration, A. A. Alves Jr. *et al.*, *The LHCb detector at the LHC*, JINST **3** (2008) S08005.

[27] LHCb collaboration, R. Aaij *et al.*, *LHCb detector performance*, Int. J. Mod. Phys. **A30** (2015) 1530022, arXiv:1412.6352.

[28] R. Aaij *et al.*, *The LHCb trigger and its performance in 2011*, JINST **8** (2013) P04022, arXiv:1211.3055.

[29] V. V. Gligorov and M. Williams, *Efficient, reliable and fast high-level triggering using a bonsai boosted decision tree*, JINST **8** (2013) P02013, arXiv:1210.6861.

[30] T. Sjöstrand, S. Mrenna, and P. Skands, *A brief introduction to PYTHIA 8.1*, Comput. Phys. Commun. **178** (2008) 852, arXiv:0710.3820.

[31] T. Sjöstrand, S. Mrenna, and P. Skands, *PYTHIA 6.4 physics and manual*, JHEP **05** (2006) 026, arXiv:hep-ph/0603175.

[32] I. Belyaev *et al.*, *Handling of the generation of primary events in Gauss, the LHCb simulation framework*, J. Phys. Conf. Ser. **331** (2011) 032047.

[33] D. J. Lange, *The EvtGen particle decay simulation package*, Nucl. Instrum. Meth. **A462** (2001) 152.

[34] P. Golonka and Z. Was, *PHOTOS Monte Carlo: A precision tool for QED corrections in Z and W decays*, Eur. Phys. J. **C45** (2006) 97, arXiv:hep-ph/0506026.

[35] Geant4 collaboration, J. Allison *et al.*, *Geant4 developments and applications*, IEEE Trans. Nucl. Sci. **53** (2006) 270; Geant4 collaboration, S. Agostinelli *et al.*, *Geant4: A simulation toolkit*, Nucl. Instrum. Meth. **A506** (2003) 250.

[36] M. Clemencic *et al.*, *The LHCb simulation application, Gauss: Design, evolution and experience*, J. Phys. Conf. Ser. **331** (2011) 032023.

[37] L. Breiman, J. H. Friedman, R. A. Olshen, and C. J. Stone, *Classification and regression trees*, Wadsworth international group, Belmont, California, USA, 1984.

[38] B. P. Roe *et al.*, *Boosted decision trees as an alternative to artificial neural networks for particle identification*, Nucl. Instrum. Meth. **A543** (2005) 577, arXiv:physics/0408124.

[39] L. Anderlini *et al.*, *The PIDCalib package*, LHCb-PUB-2016-021.

[40] N. L. Johnson, *System of frequency curves generated by methods of translation*, Biometrika **36** (1949) 149.

[41] K. S. Cranmer, *Kernel estimation in high-energy physics*, Comput. Phys. Commun. **136** (2001) 198, arXiv:hep-ex/0011057.

[42] ARGUS collaboration, H. Albrecht *et al.*, *Measurement of the polarization in the decay $B \to J/\psi K^*$*, Phys. Lett. **B340** (1994) 217.

[43] LHCb collaboration, R. Aaij *et al.*, *Measurement of B^0, B_s^0, B^+ and Λ_b^0 production asymmetries in 7 and 8 TeV pp collisions*, Phys. Lett. **B774** (2017) 139, arXiv:1703.08464.

[44] T. M. Karbach, G. Raven, and M. Schiller, *Decay time integrals in neutral meson mixing and their efficient evaluation*, arXiv:1407.0748.

[45] LHCb collaboration, R. Aaij *et al.*, *Opposite-side flavour tagging of B mesons at the LHCb experiment*, Eur. Phys. J. **C72** (2012) 2022, arXiv:1202.4979.

[46] LHCb collaboration, R. Aaij *et al.*, *New algorithms for identifying the flavour of B^0 mesons using pions and protons*, Eur. Phys. J. **C77** (2017) 238, arXiv:1610.06019.

[47] LHCb collaboration, R. Aaij *et al.*, *A new algorithm for identifying the flavour of B_s^0 mesons at LHCb*, JINST **11** (2016) P05010, arXiv:1602.07252.

[48] LHCb collaboration, R. Aaij *et al.*, *Measurement of CP asymmetry in $D^0 \to K^-K^+$ and $D^0 \to \pi^-\pi^+$ decays*, JHEP **07** (2014) 041, arXiv:1405.2797.

[49] LHCb collaboration, R. Aaij *et al.*, *Measurement of the fragmentation fraction ratio f_s/f_d and its dependence on B meson kinematics*, JHEP **04** (2013) 001, arXiv:1301.5286, f_s/f_d value updated in LHCb-CONF-2013-011.

[50] M. Pivk and F. R. Le Diberder, *sPlot: A statistical tool to unfold data distributions*, Nucl. Instrum. Meth. **A555** (2005) 356, arXiv:physics/0402083.

LHCb collaboration

R. Aaij[43], B. Adeva[39], M. Adinolfi[48], Z. Ajaltouni[5], S. Akar[59], P. Albicocco[18], J. Albrecht[10],
F. Alessio[40], M. Alexander[53], A. Alfonso Albero[38], S. Ali[43], G. Alkhazov[31],
P. Alvarez Cartelle[55], A.A. Alves Jr[59], S. Amato[2], S. Amerio[23], Y. Amhis[7], L. An[3],
L. Anderlini[17], G. Andreassi[41], M. Andreotti[16,g], J.E. Andrews[60], R.B. Appleby[56], F. Archilli[43],
P. d'Argent[12], J. Arnau Romeu[6], A. Artamonov[37], M. Artuso[61], E. Aslanides[6], M. Atzeni[42],
G. Auriemma[26], S. Bachmann[12], J.J. Back[50], S. Baker[55], V. Balagura[7,b], W. Baldini[16],
A. Baranov[35], R.J. Barlow[56], S. Barsuk[7], W. Barter[56], F. Baryshnikov[32], V. Batozskaya[29],
V. Battista[41], A. Bay[41], J. Beddow[53], F. Bedeschi[24], I. Bediaga[1], A. Beiter[61], L.J. Bel[43],
N. Beliy[63], V. Bellee[41], N. Belloli[20,i], K. Belous[37], I. Belyaev[32,40], E. Ben-Haim[8],
G. Bencivenni[18], S. Benson[43], S. Beranek[9], A. Berezhnoy[33], R. Bernet[42], D. Berninghoff[12],
E. Bertholet[8], A. Bertolin[23], C. Betancourt[42], F. Betti[15,40], M.O. Bettler[49], M. van Beuzekom[43],
Ia. Bezshyiko[42], S. Bifani[47], P. Billoir[8], A. Birnkraut[10], A. Bizzeti[17,u], M. Bjørn[57], T. Blake[50],
F. Blanc[41], S. Blusk[61], V. Bocci[26], O. Boente Garcia[39], T. Boettcher[58], A. Bondar[36,w],
N. Bondar[31], S. Borghi[56,40], M. Borisyak[35], M. Borsato[39,40], F. Bossu[7], M. Boubdir[9],
T.J.V. Bowcock[54], E. Bowen[42], C. Bozzi[16,40], S. Braun[12], M. Brodski[40], J. Brodzicka[27],
D. Brundu[22], E. Buchanan[48], C. Burr[56], A. Bursche[22], J. Buytaert[40], W. Byczynski[40],
S. Cadeddu[22], H. Cai[64], R. Calabrese[16,g], R. Calladine[47], M. Calvi[20,i], M. Calvo Gomez[38,m],
A. Camboni[38,m], P. Campana[18], D.H. Campora Perez[40], L. Capriotti[56], A. Carbone[15,e],
G. Carboni[25], R. Cardinale[19,h], A. Cardini[22], P. Carniti[20,i], L. Carson[52], K. Carvalho Akiba[2],
G. Casse[54], L. Cassina[20], M. Cattaneo[40], G. Cavallero[19,h], R. Cenci[24,p], D. Chamont[7],
M.G. Chapman[48], M. Charles[8], Ph. Charpentier[40], G. Chatzikonstantinidis[47], M. Chefdeville[4],
S. Chen[22], S.-G. Chitic[40], V. Chobanova[39], M. Chrzaszcz[40], A. Chubykin[31], P. Ciambrone[18],
X. Cid Vidal[39], G. Ciezarek[40], P.E.L. Clarke[52], M. Clemencic[40], H.V. Cliff[49], J. Closier[40],
V. Coco[40], J. Cogan[6], E. Cogneras[5], V. Cogoni[22,f], L. Cojocariu[30], P. Collins[40], T. Colombo[40],
A. Comerma-Montells[12], A. Contu[22], G. Coombs[40], S. Coquereau[38], G. Corti[40], M. Corvo[16,g],
C.M. Costa Sobral[50], B. Couturier[40], G.A. Cowan[52], D.C. Craik[58], A. Crocombe[50],
M. Cruz Torres[1], R. Currie[52], C. D'Ambrosio[40], F. Da Cunha Marinho[2], C.L. Da Silva[73],
E. Dall'Occo[43], J. Dalseno[48], A. Danilina[32], A. Davis[3], O. De Aguiar Francisco[40],
K. De Bruyn[40], S. De Capua[56], M. De Cian[41], J.M. De Miranda[1], L. De Paula[2],
M. De Serio[14,d], P. De Simone[18], C.T. Dean[53], D. Decamp[4], L. Del Buono[8], B. Delaney[49],
H.-P. Dembinski[11], M. Demmer[10], A. Dendek[28], D. Derkach[35], O. Deschamps[5], F. Dettori[54],
B. Dey[65], A. Di Canto[40], P. Di Nezza[18], S. Didenko[69], H. Dijkstra[40], F. Dordei[40], M. Dorigo[40],
A. Dosil Suárez[39], L. Douglas[53], A. Dovbnya[45], K. Dreimanis[54], L. Dufour[43], G. Dujany[8],
P. Durante[40], J.M. Durham[73], D. Dutta[56], R. Dzhelyadin[37], M. Dziewiecki[12], A. Dziurda[40],
A. Dzyuba[31], S. Easo[51], U. Egede[55], V. Egorychev[32], S. Eidelman[36,w], S. Eisenhardt[52],
U. Eitschberger[10], R. Ekelhof[10], L. Eklund[53], S. Ely[61], A. Ene[30], S. Escher[9], S. Esen[43],
H.M. Evans[49], T. Evans[57], A. Falabella[15], N. Farley[47], S. Farry[54], D. Fazzini[20,40,i], L. Federici[25],
G. Fernandez[38], P. Fernandez Declara[40], A. Fernandez Prieto[39], F. Ferrari[15], L. Ferreira Lopes[41],
F. Ferreira Rodrigues[2], M. Ferro-Luzzi[40], S. Filippov[34], R.A. Fini[14], M. Fiorini[16,g], M. Firlej[28],
C. Fitzpatrick[41], T. Fiutowski[28], F. Fleuret[7,b], M. Fontana[22,40], F. Fontanelli[19,h], R. Forty[40],
V. Franco Lima[54], M. Frank[40], C. Frei[40], J. Fu[21,q], W. Funk[40], C. Färber[40], E. Gabriel[52],
A. Gallas Torreira[39], D. Galli[15,e], S. Gallorini[23], S. Gambetta[52], M. Gandelman[2], P. Gandini[21],
Y. Gao[3], L.M. Garcia Martin[71], B. Garcia Plana[39], J. García Pardiñas[42], J. Garra Tico[49],
L. Garrido[38], D. Gascon[38], C. Gaspar[40], L. Gavardi[10], G. Gazzoni[5], D. Gerick[12],
E. Gersabeck[56], M. Gersabeck[56], T. Gershon[50], Ph. Ghez[4], S. Giani[41], V. Gibson[49],
O.G. Girard[41], L. Giubega[30], K. Gizdov[52], V.V. Gligorov[8], D. Golubkov[32], A. Golutvin[55,69],
A. Gomes[1,a], I.V. Gorelov[33], C. Gotti[20,i], E. Govorkova[43], J.P. Grabowski[12], R. Graciani Diaz[38],
L.A. Granado Cardoso[40], E. Graugés[38], E. Graverini[42], G. Graziani[17], A. Grecu[30], R. Greim[43],

P. Griffith[22], L. Grillo[56], L. Gruber[40], B.R. Gruberg Cazon[57], O. Grünberg[67], E. Gushchin[34],
Yu. Guz[37,40], T. Gys[40], C. Göbel[62], T. Hadavizadeh[57], C. Hadjivasiliou[5], G. Haefeli[41],
C. Haen[40], S.C. Haines[49], B. Hamilton[60], X. Han[12], T.H. Hancock[57], S. Hansmann-Menzemer[12],
N. Harnew[57], S.T. Harnew[48], C. Hasse[40], M. Hatch[40], J. He[63], M. Hecker[55], K. Heinicke[10],
A. Heister[9], K. Hennessy[54], L. Henry[71], E. van Herwijnen[40], M. Heß[67], A. Hicheur[2], D. Hill[57],
P.H. Hopchev[41], W. Hu[65], W. Huang[63], Z.C. Huard[59], W. Hulsbergen[43], T. Humair[55],
M. Hushchyn[35], D. Hutchcroft[54], P. Ibis[10], M. Idzik[28], P. Ilten[47], K. Ivshin[31], R. Jacobsson[40],
J. Jalocha[57], E. Jans[43], A. Jawahery[60], F. Jiang[3], M. John[57], D. Johnson[40], C.R. Jones[49],
C. Joram[40], B. Jost[40], N. Jurik[57], S. Kandybei[45], M. Karacson[40], J.M. Kariuki[48], S. Karodia[53],
N. Kazeev[35], M. Kecke[12], F. Keizer[49], M. Kelsey[61], M. Kenzie[49], T. Ketel[44], E. Khairullin[35],
B. Khanji[12], C. Khurewathanakul[41], K.E. Kim[61], T. Kirn[9], S. Klaver[18], K. Klimaszewski[29],
T. Klimkovich[11], S. Koliiev[46], M. Kolpin[12], R. Kopecna[12], P. Koppenburg[43], S. Kotriakhova[31],
M. Kozeiha[5], L. Kravchuk[34], M. Kreps[50], F. Kress[55], P. Krokovny[36,w], W. Krupa[28],
W. Krzemien[29], W. Kucewicz[27,l], M. Kucharczyk[27], V. Kudryavtsev[36,w], A.K. Kuonen[41],
T. Kvaratskheliya[32,40], D. Lacarrere[40], G. Lafferty[56], A. Lai[22], G. Lanfranchi[18],
C. Langenbruch[9], T. Latham[50], C. Lazzeroni[47], R. Le Gac[6], A. Leflat[33,40], J. Lefrançois[7],
R. Lefèvre[5], F. Lemaitre[40], O. Leroy[6], T. Lesiak[27], B. Leverington[12], P.-R. Li[63], T. Li[3], Z. Li[61],
X. Liang[61], T. Likhomanenko[68], R. Lindner[40], F. Lionetto[42], V. Lisovskyi[7], X. Liu[3], D. Loh[50],
A. Loi[22], I. Longstaff[53], J.H. Lopes[2], D. Lucchesi[23,o], M. Lucio Martinez[39], A. Lupato[23],
E. Luppi[16,g], O. Lupton[40], A. Lusiani[24], X. Lyu[63], F. Machefert[7], F. Maciuc[30], V. Macko[41],
P. Mackowiak[10], S. Maddrell-Mander[48], O. Maev[31,40], K. Maguire[56], D. Maisuzenko[31],
M.W. Majewski[28], S. Malde[57], B. Malecki[27], A. Malinin[68], T. Maltsev[36,w], G. Manca[22,f],
G. Mancinelli[6], D. Marangotto[21,q], J. Maratas[5,v], J.F. Marchand[4], U. Marconi[15],
C. Marin Benito[38], M. Marinangeli[41], P. Marino[41], J. Marks[12], G. Martellotti[26], M. Martin[6],
M. Martinelli[41], D. Martinez Santos[39], F. Martinez Vidal[71], A. Massafferri[1], R. Matev[40],
A. Mathad[50], Z. Mathe[40], C. Matteuzzi[20], A. Mauri[42], E. Maurice[7,b], B. Maurin[41],
A. Mazurov[47], M. McCann[55,40], A. McNab[56], R. McNulty[13], J.V. Mead[54], B. Meadows[59],
C. Meaux[6], F. Meier[10], N. Meinert[67], D. Melnychuk[29], M. Merk[43], A. Merli[21,q], E. Michielin[23],
D.A. Milanes[66], E. Millard[50], M.-N. Minard[4], L. Minzoni[16,g], D.S. Mitzel[12], A. Mogini[8],
J. Molina Rodriguez[1,y], T. Mombächer[10], I.A. Monroy[66], S. Monteil[5], M. Morandin[23],
G. Morello[18], M.J. Morello[24,t], O. Morgunova[68], J. Moron[28], A.B. Morris[6], R. Mountain[61],
F. Muheim[52], M. Mulder[43], D. Müller[40], J. Müller[10], K. Müller[42], V. Müller[10], P. Naik[48],
T. Nakada[41], R. Nandakumar[51], A. Nandi[57], I. Nasteva[2], M. Needham[52], N. Neri[21],
S. Neubert[12], N. Neufeld[40], M. Neuner[12], T.D. Nguyen[41], C. Nguyen-Mau[41,n], S. Nieswand[9],
R. Niet[10], N. Nikitin[33], A. Nogay[68], D.P. O'Hanlon[15], A. Oblakowska-Mucha[28], V. Obraztsov[37],
S. Ogilvy[18], R. Oldeman[22,f], C.J.G. Onderwater[72], A. Ossowska[27], J.M. Otalora Goicochea[2],
P. Owen[42], A. Oyanguren[71], P.R. Pais[41], A. Palano[14], M. Palutan[18,40], G. Panshin[70],
A. Papanestis[51], M. Pappagallo[52], L.L. Pappalardo[16,g], W. Parker[60], C. Parkes[56],
G. Passaleva[17,40], A. Pastore[14], M. Patel[55], C. Patrignani[15,e], A. Pearce[40], A. Pellegrino[43],
G. Penso[26], M. Pepe Altarelli[40], S. Perazzini[40], D. Pereima[32], P. Perret[5], L. Pescatore[41],
K. Petridis[48], A. Petrolini[19,h], A. Petrov[68], M. Petruzzo[21,q], B. Pietrzyk[4], G. Pietrzyk[41],
M. Pikies[27], D. Pinci[26], F. Pisani[40], A. Pistone[19,h], A. Piucci[12], V. Placinta[30], S. Playfer[52],
M. Plo Casasus[39], F. Polci[8], M. Poli Lener[18], A. Poluektov[50], N. Polukhina[69,c], I. Polyakov[61],
E. Polycarpo[2], G.J. Pomery[48], S. Ponce[40], A. Popov[37], D. Popov[11,40], S. Poslavskii[37],
C. Potterat[2], E. Price[48], J. Prisciandaro[39], C. Prouve[48], V. Pugatch[46], A. Puig Navarro[42],
H. Pullen[57], G. Punzi[24,p], W. Qian[63], J. Qin[63], R. Quagliani[8], B. Quintana[5], B. Rachwal[28],
J.H. Rademacker[48], M. Rama[24], M. Ramos Pernas[39], M.S. Rangel[2], F. Ratnikov[35,x],
G. Raven[44], M. Ravonel Salzgeber[40], M. Reboud[4], F. Redi[41], S. Reichert[10], A.C. dos Reis[1],
C. Remon Alepuz[71], V. Renaudin[7], S. Ricciardi[51], S. Richards[48], K. Rinnert[54], P. Robbe[7],
A. Robert[8], A.B. Rodrigues[41], E. Rodrigues[59], J.A. Rodriguez Lopez[66], A. Rogozhnikov[35],

S. Roiser[40], A. Rollings[57], V. Romanovskiy[37], A. Romero Vidal[39,40], M. Rotondo[18],
M.S. Rudolph[61], T. Ruf[40], J. Ruiz Vidal[71], J.J. Saborido Silva[39], N. Sagidova[31], B. Saitta[22,f],
V. Salustino Guimaraes[62], C. Sanchez Mayordomo[71], B. Sanmartin Sedes[39], R. Santacesaria[26],
C. Santamarina Rios[39], M. Santimaria[18], E. Santovetti[25,j], G. Sarpis[56], A. Sarti[18,k],
C. Satriano[26,s], A. Satta[25], D. Savrina[32,33], S. Schael[9], M. Schellenberg[10], M. Schiller[53],
H. Schindler[40], M. Schmelling[11], T. Schmelzer[10], B. Schmidt[40], O. Schneider[41], A. Schopper[40],
H.F. Schreiner[59], M. Schubiger[41], M.H. Schune[7], R. Schwemmer[40], B. Sciascia[18], A. Sciubba[26,k],
A. Semennikov[32], E.S. Sepulveda[8], A. Sergi[47,40], N. Serra[42], J. Serrano[6], L. Sestini[23],
P. Seyfert[40], M. Shapkin[37], Y. Shcheglov[31,†], T. Shears[54], L. Shekhtman[36,w], V. Shevchenko[68],
B.G. Siddi[16], R. Silva Coutinho[42], L. Silva de Oliveira[2], G. Simi[23,o], S. Simone[14,d],
N. Skidmore[12], T. Skwarnicki[61], I.T. Smith[52], M. Smith[55], l. Soares Lavra[1], M.D. Sokoloff[59],
F.J.P. Soler[53], B. Souza De Paula[2], B. Spaan[10], P. Spradlin[53], F. Stagni[40], M. Stahl[12],
S. Stahl[40], P. Stefko[41], S. Stefkova[55], O. Steinkamp[42], S. Stemmle[12], O. Stenyakin[37],
M. Stepanova[31], H. Stevens[10], S. Stone[61], B. Storaci[42], S. Stracka[24,p], M.E. Stramaglia[41],
M. Straticiuc[30], U. Straumann[42], S. Strokov[70], J. Sun[3], L. Sun[64], K. Swientek[28],
V. Syropoulos[44], T. Szumlak[28], M. Szymanski[63], S. T'Jampens[4], Z. Tang[3], A. Tayduganov[6],
T. Tekampe[10], G. Tellarini[16], F. Teubert[40], E. Thomas[40], J. van Tilburg[43], M.J. Tilley[55],
V. Tisserand[5], M. Tobin[41], S. Tolk[40], L. Tomassetti[16,g], D. Tonelli[24],
R. Tourinho Jadallah Aoude[1], E. Tournefier[4], M. Traill[53], M.T. Tran[41], M. Tresch[42],
A. Trisovic[49], A. Tsaregorodtsev[6], A. Tully[49], N. Tuning[43,40], A. Ukleja[29], A. Usachov[7],
A. Ustyuzhanin[35], U. Uwer[12], C. Vacca[22,f], A. Vagner[70], V. Vagnoni[15], A. Valassi[40], S. Valat[40],
G. Valenti[15], R. Vazquez Gomez[40], P. Vazquez Regueiro[39], S. Vecchi[16], M. van Veghel[43],
J.J. Velthuis[48], M. Veltri[17,r], G. Veneziano[57], A. Venkateswaran[61], T.A. Verlage[9], M. Vernet[5],
M. Vesterinen[57], J.V. Viana Barbosa[40], D. Vieira[63], M. Vieites Diaz[39], H. Viemann[67],
X. Vilasis-Cardona[38,m], A. Vitkovskiy[43], M. Vitti[49], V. Volkov[33], A. Vollhardt[42], B. Voneki[40],
A. Vorobyev[31], V. Vorobyev[36,w], C. Voß[9], J.A. de Vries[43], C. Vázquez Sierra[43], R. Waldi[67],
J. Walsh[24], J. Wang[61], M. Wang[3], Y. Wang[65], Z. Wang[42], D.R. Ward[49], H.M. Wark[54],
N.K. Watson[47], D. Websdale[55], A. Weiden[42], C. Weisser[58], M. Whitehead[9], J. Wicht[50],
G. Wilkinson[57], M. Wilkinson[61], M.R.J. Williams[56], M. Williams[58], T. Williams[47],
F.F. Wilson[51,40], J. Wimberley[60], M. Winn[7], J. Wishahi[10], W. Wislicki[29], M. Witek[27],
G. Wormser[7], S.A. Wotton[49], K. Wyllie[40], D. Xiao[65], Y. Xie[65], A. Xu[3], M. Xu[65], Q. Xu[63],
Z. Xu[3], Z. Xu[4], Z. Yang[3], Z. Yang[60], Y. Yao[61], H. Yin[65], J. Yu[65,z], X. Yuan[61],
O. Yushchenko[37], K.A. Zarebski[47], M. Zavertyaev[11,c], L. Zhang[3], Y. Zhang[7], A. Zhelezov[12],
Y. Zheng[63], X. Zhu[3], V. Zhukov[9,33], J.B. Zonneveld[52], S. Zucchelli[15].

[1] *Centro Brasileiro de Pesquisas Físicas (CBPF), Rio de Janeiro, Brazil*
[2] *Universidade Federal do Rio de Janeiro (UFRJ), Rio de Janeiro, Brazil*
[3] *Center for High Energy Physics, Tsinghua University, Beijing, China*
[4] *Univ. Grenoble Alpes, Univ. Savoie Mont Blanc, CNRS, IN2P3-LAPP, Annecy, France*
[5] *Clermont Université, Université Blaise Pascal, CNRS/IN2P3, LPC, Clermont-Ferrand, France*
[6] *Aix Marseille Univ, CNRS/IN2P3, CPPM, Marseille, France*
[7] *LAL, Univ. Paris-Sud, CNRS/IN2P3, Université Paris-Saclay, Orsay, France*
[8] *LPNHE, Université Pierre et Marie Curie, Université Paris Diderot, CNRS/IN2P3, Paris, France*
[9] *I. Physikalisches Institut, RWTH Aachen University, Aachen, Germany*
[10] *Fakultät Physik, Technische Universität Dortmund, Dortmund, Germany*
[11] *Max-Planck-Institut für Kernphysik (MPIK), Heidelberg, Germany*
[12] *Physikalisches Institut, Ruprecht-Karls-Universität Heidelberg, Heidelberg, Germany*
[13] *School of Physics, University College Dublin, Dublin, Ireland*
[14] *INFN Sezione di Bari, Bari, Italy*
[15] *INFN Sezione di Bologna, Bologna, Italy*
[16] *INFN Sezione di Ferrara, Ferrara, Italy*
[17] *INFN Sezione di Firenze, Firenze, Italy*

[18] INFN Laboratori Nazionali di Frascati, Frascati, Italy

[19] INFN Sezione di Genova, Genova, Italy

[20] INFN Sezione di Milano-Bicocca, Milano, Italy

[21] INFN Sezione di Milano, Milano, Italy

[22] INFN Sezione di Cagliari, Monserrato, Italy

[23] INFN Sezione di Padova, Padova, Italy

[24] INFN Sezione di Pisa, Pisa, Italy

[25] INFN Sezione di Roma Tor Vergata, Roma, Italy

[26] INFN Sezione di Roma La Sapienza, Roma, Italy

[27] Henryk Niewodniczanski Institute of Nuclear Physics Polish Academy of Sciences, Kraków, Poland

[28] AGH - University of Science and Technology, Faculty of Physics and Applied Computer Science, Kraków, Poland

[29] National Center for Nuclear Research (NCBJ), Warsaw, Poland

[30] Horia Hulubei National Institute of Physics and Nuclear Engineering, Bucharest-Magurele, Romania

[31] Petersburg Nuclear Physics Institute (PNPI), Gatchina, Russia

[32] Institute of Theoretical and Experimental Physics (ITEP), Moscow, Russia

[33] Institute of Nuclear Physics, Moscow State University (SINP MSU), Moscow, Russia

[34] Institute for Nuclear Research of the Russian Academy of Sciences (INR RAS), Moscow, Russia

[35] Yandex School of Data Analysis, Moscow, Russia

[36] Budker Institute of Nuclear Physics (SB RAS), Novosibirsk, Russia

[37] Institute for High Energy Physics (IHEP), Protvino, Russia

[38] ICCUB, Universitat de Barcelona, Barcelona, Spain

[39] Instituto Galego de Física de Altas Enerxías (IGFAE), Universidade de Santiago de Compostela, Santiago de Compostela, Spain

[40] European Organization for Nuclear Research (CERN), Geneva, Switzerland

[41] Institute of Physics, Ecole Polytechnique Fédérale de Lausanne (EPFL), Lausanne, Switzerland

[42] Physik-Institut, Universität Zürich, Zürich, Switzerland

[43] Nikhef National Institute for Subatomic Physics, Amsterdam, The Netherlands

[44] Nikhef National Institute for Subatomic Physics and VU University Amsterdam, Amsterdam, The Netherlands

[45] NSC Kharkiv Institute of Physics and Technology (NSC KIPT), Kharkiv, Ukraine

[46] Institute for Nuclear Research of the National Academy of Sciences (KINR), Kyiv, Ukraine

[47] University of Birmingham, Birmingham, United Kingdom

[48] H.H. Wills Physics Laboratory, University of Bristol, Bristol, United Kingdom

[49] Cavendish Laboratory, University of Cambridge, Cambridge, United Kingdom

[50] Department of Physics, University of Warwick, Coventry, United Kingdom

[51] STFC Rutherford Appleton Laboratory, Didcot, United Kingdom

[52] School of Physics and Astronomy, University of Edinburgh, Edinburgh, United Kingdom

[53] School of Physics and Astronomy, University of Glasgow, Glasgow, United Kingdom

[54] Oliver Lodge Laboratory, University of Liverpool, Liverpool, United Kingdom

[55] Imperial College London, London, United Kingdom

[56] School of Physics and Astronomy, University of Manchester, Manchester, United Kingdom

[57] Department of Physics, University of Oxford, Oxford, United Kingdom

[58] Massachusetts Institute of Technology, Cambridge, MA, United States

[59] University of Cincinnati, Cincinnati, OH, United States

[60] University of Maryland, College Park, MD, United States

[61] Syracuse University, Syracuse, NY, United States

[62] Pontifícia Universidade Católica do Rio de Janeiro (PUC-Rio), Rio de Janeiro, Brazil, associated to [2]

[63] University of Chinese Academy of Sciences, Beijing, China, associated to [3]

[64] School of Physics and Technology, Wuhan University, Wuhan, China, associated to [3]

[65] Institute of Particle Physics, Central China Normal University, Wuhan, Hubei, China, associated to [3]

[66] Departamento de Fisica , Universidad Nacional de Colombia, Bogota, Colombia, associated to [8]

[67] Institut für Physik, Universität Rostock, Rostock, Germany, associated to [12]

[68] National Research Centre Kurchatov Institute, Moscow, Russia, associated to [32]

[69] National University of Science and Technology "MISIS", Moscow, Russia, associated to [32]

[70] National Research Tomsk Polytechnic University, Tomsk, Russia, associated to [32]

[71] *Instituto de Fisica Corpuscular, Centro Mixto Universidad de Valencia - CSIC, Valencia, Spain, associated to [38]*

[72] *Van Swinderen Institute, University of Groningen, Groningen, The Netherlands, associated to [43]*

[73] *Los Alamos National Laboratory (LANL), Los Alamos, United States, associated to [61]*

[a] *Universidade Federal do Triângulo Mineiro (UFTM), Uberaba-MG, Brazil*

[b] *Laboratoire Leprince-Ringuet, Palaiseau, France*

[c] *P.N. Lebedev Physical Institute, Russian Academy of Science (LPI RAS), Moscow, Russia*

[d] *Università di Bari, Bari, Italy*

[e] *Università di Bologna, Bologna, Italy*

[f] *Università di Cagliari, Cagliari, Italy*

[g] *Università di Ferrara, Ferrara, Italy*

[h] *Università di Genova, Genova, Italy*

[i] *Università di Milano Bicocca, Milano, Italy*

[j] *Università di Roma Tor Vergata, Roma, Italy*

[k] *Università di Roma La Sapienza, Roma, Italy*

[l] *AGH - University of Science and Technology, Faculty of Computer Science, Electronics and Telecommunications, Kraków, Poland*

[m] *LIFAELS, La Salle, Universitat Ramon Llull, Barcelona, Spain*

[n] *Hanoi University of Science, Hanoi, Vietnam*

[o] *Università di Padova, Padova, Italy*

[p] *Università di Pisa, Pisa, Italy*

[q] *Università degli Studi di Milano, Milano, Italy*

[r] *Università di Urbino, Urbino, Italy*

[s] *Università della Basilicata, Potenza, Italy*

[t] *Scuola Normale Superiore, Pisa, Italy*

[u] *Università di Modena e Reggio Emilia, Modena, Italy*

[v] *MSU - Iligan Institute of Technology (MSU-IIT), Iligan, Philippines*

[w] *Novosibirsk State University, Novosibirsk, Russia*

[x] *National Research University Higher School of Economics, Moscow, Russia*

[y] *Escuela Agrícola Panamericana, San Antonio de Oriente, Honduras*

[z] *Physics and Micro Electronic College, Hunan University, Changsha City, China*

[†] *Deceased*